Active control of arousal by a locus coeruleus GABAergic circuit

Vincent Breton-Provencher and Mriganka Sur ⓘ *

Arousal responses linked to locus coeruleus noradrenergic (LC-NA) activity affect cognition. However, the mechanisms that control modes of LC-NA activity remain unknown. Here, we reveal a local population of GABAergic neurons (LC-GABA) capable of modulating LC-NA activity and arousal. Retrograde tracing shows that inputs to LC-GABA and LC-NA neurons arise from similar regions, though a few regions provide differential inputs to one subtype over the other. Recordings in the locus coeruleus demonstrate two modes of LC-GABA responses whereby spiking is either correlated or broadly anticorrelated with LC-NA responses, reflecting anatomically similar and functionally coincident inputs, or differential and non-coincident inputs, to LC-NA and LC-GABA neurons. Coincident inputs control the gain of LC-NA-mediated arousal responses, whereas non-coincident inputs, such as from the prefrontal cortex to the locus coeruleus, alter global arousal levels. These findings demonstrate distinct modes by which an inhibitory locus coeruleus circuit regulates arousal in the brain.

Noradrenergic (NA) neurons located in the locus coeruleus (LC) send broad projections to a wide variety of brain regions, and their activity correlates with levels of arousal and cognitive performance[1–6]. During wakefulness, fluctuations in LC-NA arousal modify plasticity[7], shift attention[3,8], induce anxiety[9], or affect discrimination and general sensory perception[10–13]. Even though the effect of NA-mediated arousal on brain processing has become clearer in recent years, we still have a poor understanding of the mechanisms that regulate NA activity.

LC neurons receive inputs from a large number of brain regions[14], which probably underlies the diverse contexts that drive LC-NA neuronal activity, including sensory stimuli and stressors[15–19]. In particular, LC neurons are thought to be novelty detectors, as NA release increases in response to novel sensory stimuli and with stimulus saliency[7,19,20]. The novelty response also changes with learning, suggesting that distinct mechanisms suppress or promote LC-NA-mediated arousal[17,20]. Alongside these mechanisms regulating phasic LC responses, the modulation of tonic LC activity can also occur over longer timescales, such as during different levels of vigilance[21], or during environmental changes[7] or goal-directed behaviors[22]. Tight regulation of the global level of arousal has a key role in brain processing, as unregulated arousal leads to hyperanxiety and detrimental performance[12,23]. One hypothesis to explain how LC responses are modulated is that local inhibition has an active role in controlling LC-NA tonic activity and phasic responses. Consistent with this idea, previous ex vivo reports using ultrastructural microscopy and slice recordings have shown that LC neurons receive direct GABAergic inputs, and it has been speculated that this inhibitory contribution originates from local GABAergic (LC-GABA) neurons[24,25]. Recordings across sleep-wake cycles have shown that GABA neurons in or near the LC are modulated during the sleep-wake cycle, similar to LC-NA neurons[26,27]. However, there has been no study of the location or function of LC-GABA neurons, the inputs they receive, or how they modulate LC-NA activity in the awake animal.

Here, we used a combination of anatomical, electrophysiological, and optogenetic tools to identify the location, inputs, and function of a local population of LC-GABA neurons in mice, and the mode by which they control LC-NA neurons. We found that the pattern of inputs to LC-GABA neurons allows two modes of inhibition of LC-NA activity: coincident inputs to LC-NA and LC-GABA neurons regulate the gain of phasic NA responses, whereas non-coincident inputs, such as preferential inputs from the prefrontal cortex (PFC) to LC-GABA neurons, regulate LC-NA tonic activity. Together, our findings identify a mechanism by which NA-mediated arousal is selectively modulated in the brain.

Results

Location of GABAergic neurons of the LC. Previous electron microscopy ultrastructural studies have proposed the existence of GABAergic neurons surrounding LC[24]. However, a clear map of the location of GABA neurons with respect to LC-NA neurons is lacking. To mark the precise location of LC-NA neurons, we injected dopamine-beta-hydroxylase-Cre (*Dbh-Cre*) mice with a Flex-tdTomato virus and examined coronal sections of the entire LC (Fig. 1a). We used immunohistochemical staining against GABA to localize LC-GABA neurons (Fig. 1b) and marked the location of LC-GABA with respect to LC-NA neurons in each mouse (Fig. 1c). Quantification of neuronal density in the LC region revealed a greater density of LC-GABA neurons in the anterior and medial parts of the LC (Fig. 1d,e). Overall, we observed that GABA neurons intermingled with and surround NA neurons in the LC.

We next examined whether these local GABA neurons contact LC-NA neurons. To target LC-GABA neurons, we injected the LC of *Gad2-IRES-Cre* mice with Cre-dependent Flox-mCherry viruses. Quantification of Gad2-Cre-expressing neurons with markers for GABA showed an average of $87 \pm 1\%$ and $86 \pm 2\%$ of cells coexpressing either GABA or GAD67, respectively (Supplementary Fig. 1a,b,e). In contrast, the expression of *Gad2-Cre* in tyrosine hydroxylase (TH)-positive somas was $0.4 \pm 0.2\%$ and in neuropeptide-S-expressing neurons, which have been shown to be expressed in a subset of LC neurons[28], $0.8 \pm 0.8\%$ (Supplementary Fig. 1c–e). GABAergic processes entering the LC-NA region were apposed to TH-expressing somas, and staining against the vesicular GABAergic
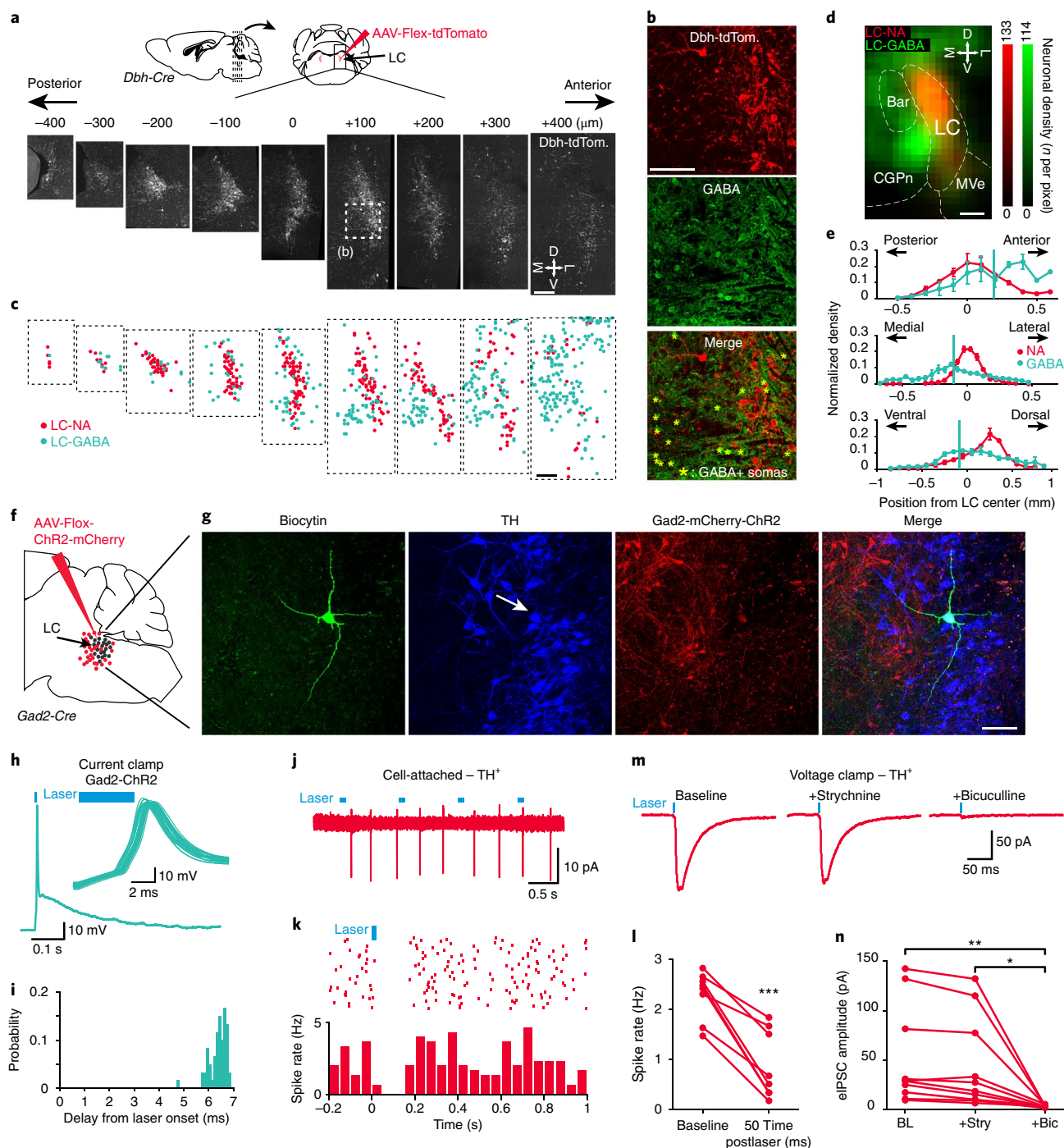
Picower Institute for Learning and Memory, Department of Brain and Cognitive Sciences, Massachusetts Institute of Technology, Cambridge, MA, USA.
*e-mail: msur@mit.edu

Fig. 1 | GABAergic neurons surround and contact LC-NA neurons. a, *Dbh-Cre* mice were injected with AAV-Flex-tdTomato virus in the LC and coronal sections were collected. The boxed area (at +100-μm location) is shown magnified in **b**. *Dbh*-tdTom., *Dbh-Cre* dependent tdTomato expression; M, medial; D, dorsal; L, lateral; V, ventral. **b**, Locations of GABA-expressing somas were revealed by immunohistochemistry. **c**, LC-NA and LC-GABA soma locations derived from **a** and **b**. **d**, Map of LC-GABA and LC-NA neuronal density in a radius of 200 μm around the LC region. The map is projected onto an antero-posterior axis. Bar, Barrington's nucleus; MVe, medial vestibular nucleus; CGPn, central gray of the pons. **e**, Distributions of LC-GABA and LC-NA neurons in the three axes. Vertical green lines represent the center of the distribution for the GABA+ population. Data are presented as mean ± s.e.m. *N* = 3 mice used for **a–e**. **f**, Methods for infecting LC-GABA neurons with mCherry/ChR2. **g**, Example of an LC neuron filled with biocytin during whole-cell recordings that expressed TH (arrow). Repeated for eight LC neurons. **h**, Current-clamp recording of a *Gad2-mCherry*-expressing neuron. Inset, overlay of multiple trials of the same cell following light activation. **i**, Distribution of spike delays from light onset of the cell shown in **h**. **j,k**, Example traces from the LC-TH+ neurons displayed in **g**. **j**, Cell-attached recordings during light activation of *Gad2* neurons. **k**, Raster plot and poststimulus time histogram aligned to light activation. **l**, Effect of light activation on spike rates for all TH+ neurons recorded (*n* = 8 neurons from 3 mice, ***P* = 0.00015, two-tailed paired *t* test, $t_7 = -6.5869$). **m**, Trial average (*n* = 60 trials) IPSCs recorded in voltage clamp following light activation and the application of strychnine and bicuculline. **n**, Light-evoked IPSC amplitudes following application of strychnine and bicuculline (*n* = 10 neurons from 4 mice, one-way repeated measures ANOVA, $F_{2,9} = 8.601$, ***P* = 0.0034, ***P* = 0.0102 using Tukey post hoc test). Blue bars in **h** and **j–l** indicate the timing of blue light activation. BL, baseline; +Stry, strychnine; +Bic, bicuculline. Scale bars represent 200 μm (**a,c**, and **d**) and 100 μm (**b** and **g**).

transporter (VGAT) revealed the existence of GABAergic contacts (Supplementary Fig. 1f,g).

To directly assess inhibitory synapses between LC-GABA and LC-NA neurons, we performed acute slice electrophysiological recordings in the LC of *Gad2-Cre* mice injected with Flox-ChR2 virus (Fig. 1f). Patched neurons were filled with biocytin during whole-cell recording and identified as LC-NA neurons by post hoc immunohistochemistry against TH (Fig. 1g). Current-clamp recordings from Gad2-mCherry-ChR2-expressing neurons showed that a 5-ms pulse of blue light was sufficient to elicit a single action potential at short latency (5 of 5 Gad2-ChR2 neurons recorded) (Fig. 1h,i). Activation of *Gad2-ChR2* neurons significantly decreased the spontaneous firing activity of TH-expressing LC-NA neurons, recorded in cell-attached mode (Fig. 1j–l). To assess the synaptic basis of this inhibition, we monitored blue light-evoked inhibitory postsynaptic currents (IPSCs) in TH neurons by performing whole-cell voltage-clamp recordings in these cells. Baseline recording with bath application of D-2-amino-5-phosphonovaleric acid (D-AP5) and 6-cyano-7-nitroquinoxaline-2 (CNQX), to block fast glutamatergic synaptic transmission, showed an average IPSC amplitude of -50.5 ± 15.8 pA (Fig. 1m,n). Blocking glycinergic transmission with strychnine had no effect on the IPSC, but applying bicuculline, a GABA$_A$ receptor antagonist, abolished the current (Fig. 1m,n). These results thus show that a dense population of GABAergic neurons located in the LC region forms functional synaptic contacts with and inhibits LC-NA neurons.

LC-GABA neurons reduce LC-NA-mediated arousal. To test whether LC-GABA neurons affect LC-mediated arousal, we first established the relationship between LC-NA activity and pupil size of awake head-restrained mice (Fig. 2a,b). We examined whether pupil size correlates with NA activity using two-photon imaging of axons filled with the genetically encoded calcium indicator GCaMP6s in the visual cortex and PFC of *Dbh-Cre* and *TH-Cre* mice (Supplementary Fig. 2a,b). We found that NA activity correlated positively with pupil size and increased before pupil dilation events (Supplementary Fig. 2c–f). We also confirmed these data with photo-identification of singleunit recording in the LC of *Dbh-Cre* animals expressing Flox-ChR2 (Supplementary Fig. 2g,h). As an additional indicator of arousal, we examined body movement along with pupil size and found a tight correlation between the two measures (Supplementary Fig. 3). This finding is consistent with previous studies, which have shown that pupil size reflects LC neuronal activity[1,5,6]. It also confirms the relationship between LC-NA activity, pupil size, and global increase in arousal as previously measured with electroencephalogram (EEG) and cortical local field potential (LFP) recordings[4,6,10–12]. We thus consider pupil size to be a useful measure of NA-mediated arousal.

To demonstrate causality between NA activity and pupil size, we injected a Flox-ChR2-mCherry virus bilaterally in the LC of *Dbh-Cre* mice (Fig. 2c), implanted optic fibers connected to a solid-state laser light source in the LC of both hemispheres (Fig. 2c,d), and applied pulsed blue light to mimic the observed increase in LC-NA activity preceding pupil dilation, as recorded in photo-tagged LC-NA units (Supplementary Fig. 2g,h). As hypothesized from NA axonal imaging, we observed a robust increase in pupil size after light activation of ChR2-expressing NA neurons (Fig. 2e,h). Pupil dilation was dependent on baseline pupil size, as activating LC-NA neurons in periods of already increased arousal produced smaller increases in pupil size, thus explaining the observed trial-to-trial variability (Supplementary Fig. 4a,b). Even moderate activation of LC-NA neurons (pulse train duration of 0.1 s at a frequency of 5 Hz) was sufficient to dilate the pupil, and this dilation increased with higher intensities of light activation (Supplementary Fig. 4c,d). We did not observe pupil dilation in control experiments using similar patterns of light activation in *Dbh-Cre* mice expressing only a fluorescent marker (Flex-tdTomato) (Fig. 2h).

Subsequently, we optically silenced LC-NA neurons to examine whether their activity was necessary for pupil dilation. After injection of Flex-ArchT-mCherry virus in *Dbh-Cre* mice and implantation of optic fibers, we silenced spontaneous LC-NA activity with green light, and observed pupil constriction (Fig. 2f,i). Although all of the *Dbh-ArchT* mice showed pupil constriction with light, this constriction was not observed in mice expressing the fluorophore alone (Fig. 2i). These results demonstrate that LC-NA activity is sufficient to alter pupil dilation and that a change in NA activity is reliably reflected in pupil size.

Our anatomical and slice electrophysiological results suggest that local LC-GABA neurons are positioned to inhibit LC-NA neurons. We tested this hypothesis by implanting an optic fiber over the LC in *Gad2-Cre* mice locally injected with Flox-ChR2 or *VGAT-YFP-ChR2*, in which all inhibitory neurons express ChR2[29]. Light activation produced a decrease in pupil size following focal stimulation, which was not observed in control animals (Fig. 2g,j). Overall, these results demonstrate that local GABA neurons in the LC control the activity of NA neurons and arousal level as reflected in pupil size.

Inputs to LC-GABA and LC-NA neurons. To further understand the function of LC-GABA neurons with respect to LC-NA neurons, we targeted a modified rabies virus separately to each subpopulation to examine the anatomical sources of their presynaptic inputs[30]. We injected two Cre-dependent (AAV) 'helper' viruses to express the avian-specific retroviral receptor (TVA) and the rabies glycoprotein in *Gad2-Cre* or *Dbh-Cre* mice. Three weeks after the first injection, we injected the modified rabies virus (rabies-deleted-glycoprotein-mCherry$^+$EnvA) that only infected cells expressing TVA and spread only from cells expressing the glycoprotein (Fig. 3a). We waited an additional week and examined coronal sections of the entire brain. Both experiments showed neurons positive for mCherry in a wide range of locations (Fig. 3b,c and Supplementary Table 1). We counted input neurons and assigned them to different brain regions. To visualize the projection patterns to LC-GABA and LC-NA neurons, we created a map of the relative contribution of each brain region to the two subpopulations (Fig. 3d,e, showing regions with >0.5% total inputs). Brain regions contacting LC-NA neurons directly were similar to those reported previously, consisting of diverse structures related to sensory, cognitive, autonomic, and motor functions[14,31,32] (Fig. 3d). Nearly all of the approximately 50 regions providing input to LC-NA neurons also projected to LC-GABA neurons (Supplementary Table 1 and Fig. 3e). However, there were variations in the extent of projections; mapping the differential contribution of input regions to the two LC neuron subtypes showed seven core regions projecting preferentially to LC-GABA versus two regions to LC-NA neurons (Fig. 3f). Thus, these findings demonstrate that the two neuronal subtypes in the LC receive largely similar inputs, whereas a few regions provide preferential input to one neuronal subtype or another.

Two types of arousal-related neuronal activity in the LC. To understand how LC-NA and LC-GABA neurons integrate their inputs to influence arousal levels in the brain, we recorded from *Dbh*- and *Gad2*-expressing neurons identified with optogenetics (photo-tagging). *Dbh-Cre* or *Gad2-Cre* mice were injected with a *Flox-ChR2* virus, and light-activated neurons were recorded with a 16-channel silicon probe equipped with an optic fiber connected to a laser source (Fig. 4a). The probe was coated with 1,1'-dioctadecyl-3,3,3',3'-tetramethylindocarbocyanine perchlorate (DiI) crystals to verify the recording location, together with immunohistochemistry against TH to identify the LC, after each successful session (Fig. 4b). Using this multichannel probe and automated spike sorting, we isolated single units from our extracellular recordings (Fig. 4c). Brief laser pulses (<5 ms) were applied and units responding to laser pulses with a short delay (<10 ms) were identified as
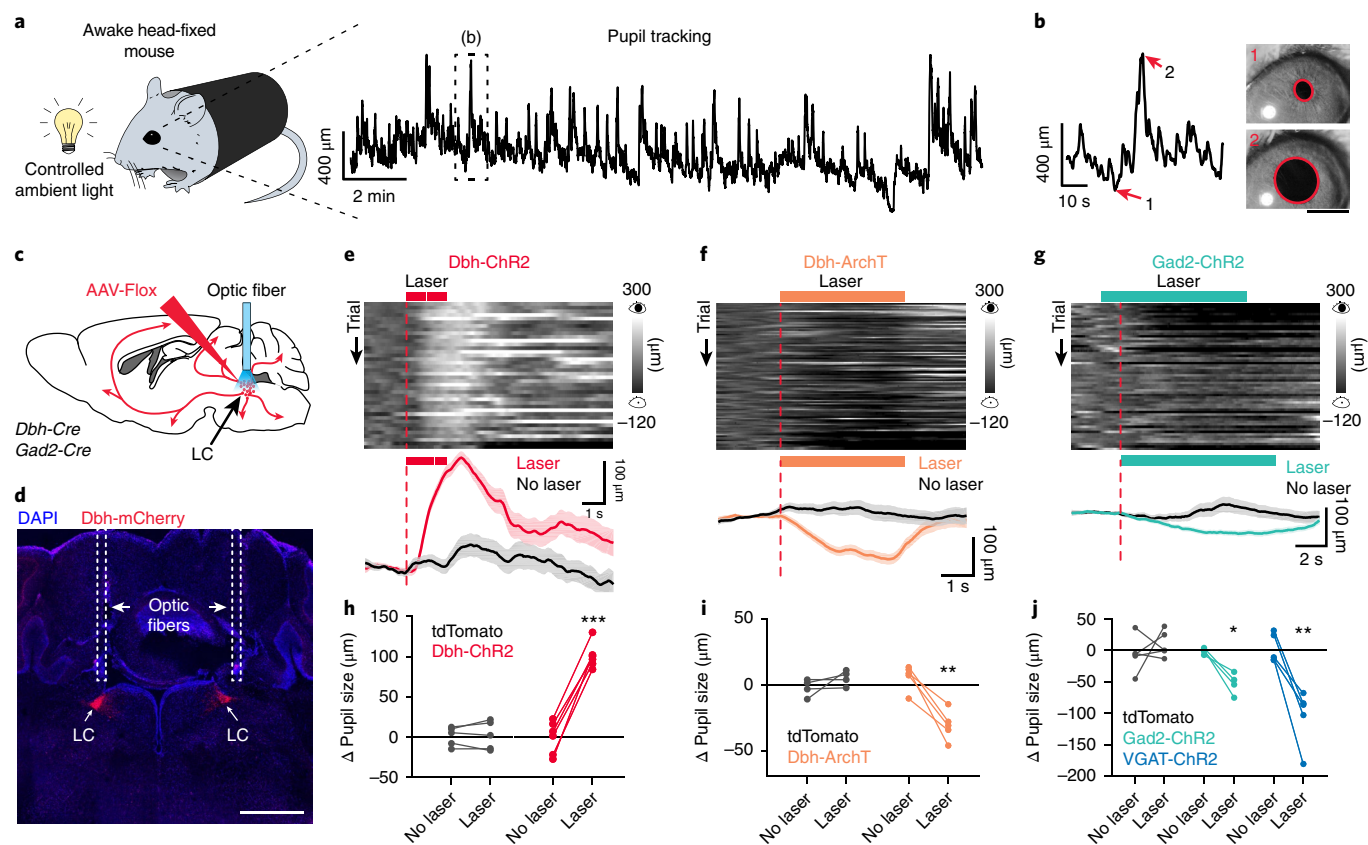
Fig. 2 | Activating LC-GABA neurons reduces LC-NA-mediated pupil size. a, Methods to measure pupil size in awake head-fixed mice using a complementary metal oxide semiconductor (CMOS) camera and infrared illumination. Right, pupil diameter for an example 20-min session. Boxed area is expanded in **b**. **b**, Example images of pupil tracking for constricted (1) and dilated (2) epochs. Scale bar represents 1 mm. **c**, Methods for optogenetic manipulation of LC-NA and LC-GABA neurons using Cre-dependent viruses, *Dbh-* and *Gad2-Cre* mice, and fiber optic implantation. **d**, Coronal section of the LC showing ChR2-mCherry expression and optic fiber tracks in a *Dbh-Cre* mouse. Scale bar represents 1 mm. **e–g**, Effect of activating (*Dbh-ChR2*) or silencing (*Dbh-ArchT*) LC-NA neurons as well as activating LC-GABA neurons (*Gad2-ChR2*) on pupil size in example mice. Top panels, temporal raster plots of pupil size aligned to optical activation onset (vertical red line). Bottom panels, session averages for trials with and without laser. Data are presented as mean ± s.e.m. **h–j**, Effect of activating or silencing LC-NA neurons as well as activating LC-GABA neurons on pupil size. Gray lines represent animals where only tdTomato was expressed, but similar optical activation patterns and intensities were used. $N = 6, 5, 4,$ and 5 mice for *Dbh*-ChR2, ArchT, *Gad2*-ChR2, and *VGAT-ChR2* conditions, respectively. $N = 5$ mice for tdTomato controls. Paired two-tailed t test with $P = 0.822$ ($t_4 = 0.240$) and ***$P = 0.00001$ ($t_5 = 14.553$) for tdTomato and ChR2 conditions in **h**; $P = 0.249$ ($t_3 = 1.426$) and **$P = 0.0045$ ($t_4 = -5.768$) for tdTomato and ArchT conditions in **i**; $P = 0.4747$ ($t_4 = 0.788$), **$P = 0.0054$ ($t_4 = -5.494$), and *$P = 0.0153$ ($t_3 = -5.010$) for tdTomato, *VGAT-ChR2*, and *Gad2*-ChR2 conditions in **j**.

expressing either *Dbh-ChR2* or *Gad2-* (Fig. 4d,e). Of 433 units recorded in 21 sessions from 13 mice, 19 *Dbh-ChR2* and 18 *Gad2-ChR2* units were photo-tagged using this method (Fig. 4f–j). The delay and jitter of light-elicited spikes were similar for the *Dbh-* and *Gad2-ChR2* conditions (Fig. 4f,g). The *Gad2* units showed higher levels of spontaneous activity and had shorter spike durations than the *Dbh* units (Fig. 4h–j).

We next examined the relationship of *Dbh-* and *Gad2-ChR2* photo-tagged units to pupil size (Fig. 5a). As expected from the axonal calcium imaging data from LC-NA neurons (Supplementary Fig. 2a–f) and from responses of photo-tagged LC-NA units (Supplementary Fig. 2g,h), pupil dilation was associated with an increase in activity of photo-tagged *Dbh-ChR2* units. In contrast, the activity of *Gad2-ChR2* units was more heterogeneous, with individual units showing negative or positive correlation with pupil size (Fig. 5a). The Pearson correlation coefficient between firing rates of LC units and pupil size (Fig. 5b) showed that all *Dbh* units correlated positively with pupil size (Fig. 5b,c). This matched the correlation recorded with two-photon calcium imaging of LC-NA axons in the cortex (Supplementary Fig. 2c) On the other hand, *Gad2* units correlated both positively (Gad2+) and negatively (Gad2−) with

pupil size (61% and 33% of *Gad2* units, respectively; Fig. 5c). The activity of Gad2− neurons globally increased during periods of low pupil constriction, whereas Gad2+ and *Dbh* neurons increased their activity during pupil dilation (Fig. 5d).

We also examined the relationship of 396 units, which were recorded in the same mice, but were not photo-tagged, to pupil dilation (Fig. 5b). We classified these units as fast spiking (FS) or regular spiking based on their spike shape, and extracted two clusters by fitting a Gaussian mixture model to the data (Supplementary Fig. 5a). The FS and regular-spiking clusters overlapped the spikes recorded in *Gad2* and *Dbh-Cre* mice (11 of 18 and 17 of 19 overlap between *Gad2* and FS, and *Dbh* and regular-spiking neurons, respectively). Spike shapes of some *Gad2* neurons were not well separated from Dbh neurons, demonstrating the difficulty of cell-type identification based on spike shape alone[33]. Still, as for photo-tagged *Dbh* and *Gad2* units, regular-spiking units were positively correlated with pupil size, whereas FS units were both positively (FS+) and negatively (FS−) correlated in similar proportion to Gad2+ and Gad2− neurons (Supplementary Fig. 5b–e), indicating a robust classification of these neuron types based on their pupillary effects.
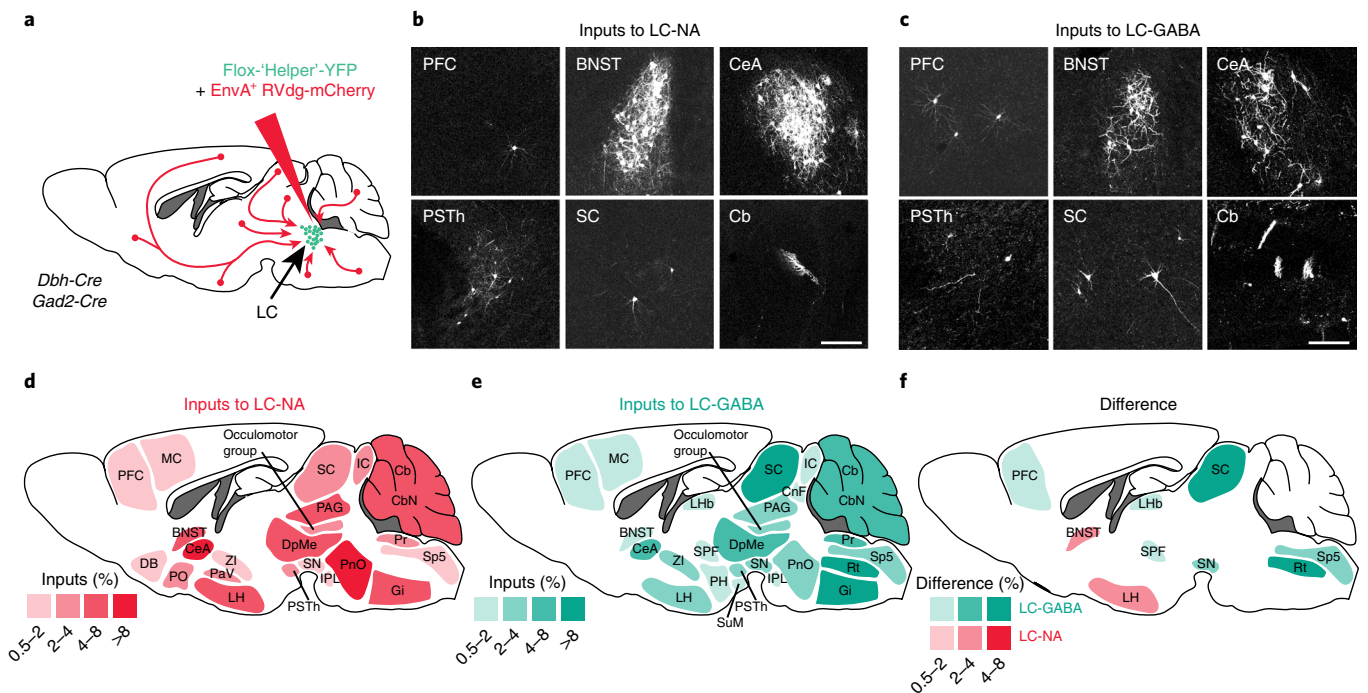
Fig. 3 | LC-NA and LC-GABA neurons receive inputs from similar as well as different sources. a, Schematic for targeting pseudo-rabies virus to LC-NA and LC-GABA subpopulations. **b,c**, Transsynaptically labeled neurons in different brain regions following injection of targeted pseudo-rabies virus in LC of *Dbh-Cre* or *Gad2-Cre* mice. Repeated in *N* = 8 and 4 mice for LC-NA and GABA, respectively. Scale bars represent 200 µm. **d,e**, Map of brain regions providing the largest fraction of inputs to LC-NA and LC-GABA neurons. Regions providing less than 0.5% of total inputs are not displayed. *N* = 8 and 4 mice for LC-NA and LC-GABA, respectively. **f**, Map of the difference in inputs to LC-NA and LC-GABA neurons. Only regions showing significant difference are displayed (*P* < 0.05 using paired *t* test; see Supplementary Table 1). BNST, bed nucleus of the stria terminalis; Cb, cerebellum; CbN, cerebellar nuclei; CnF, cuneiform nucleus; DB, diagonal band; DpMe, deep mesencephalic nucleus; Gi, gigantocellular nucleus; IC, inferior colliculus; IPL, interpeduncular nucleus; LH, lateral hypothalamus; LHb, lateral habenular nucleus; MC, motor cortex; PAG, periaqueductal gray; PaV, paraventricular nucleus; PH, posterior hypothalamus; PnO, pontine nucleus; PO, preoptic nucleus; Pr, prepositus nucleus; PSTh, parasubthalamic nucleus; Rt, reticular nucleus; SC, superior colliculus; SN, substantia nigra; Sp5, spinal trigeminal tract; SPF, subparafascicular thalamic nucleus; SuM, supramammillary nucleus; ZI, zona incerta.

We examined more closely the effect of the different types of units on pupil dilation by calculating the cross-correlation between spike rate and pupil size (Fig. 5e). The peak in cross-correlation for *Dbh* and Gad2⁺ units overlapped, whereas the Gad2⁻ units showed a broad trough in cross-correlation (Fig. 5e,f; see also Supplementary Fig. 5f,g). To get a better understanding of the timing of different LC units, we aligned their activity to dilation events (Supplementary Fig. 6a). *Dbh* and Gad2⁺ units showed a significant increase in their activity preceding dilation, whereas Gad2⁻ units showed no significant modulation in activity during dilation (Supplementary Fig. 6b,c). As a net effect, Gad2⁺ and *Dbh* activity correlated tightly during dilation and arousal, whereas Gad2⁻ activity was broadly anticorrelated to the rest of LC activity. These two types of *Gad2* units did not differ in their spontaneous firing rate, their waveform duration, or their light-evoked response (Supplementary Fig. 7). Thus, Gad2⁺ and Gad2⁻ units do not necessarily represent separate subpopulations of interneurons based on their firing properties, but rather subpopulations that differ in the inputs they receive. Hence, brain regions targeting both LC-GABA and LC-NA neurons (for example, LH, central amygdala (CeA), deep mesencephalic nucleus, pontine nucleus, or gigantocellular nucleus) would provide inputs to Gad2⁺ neurons (Fig. 3d,e), whereas Gad2⁻ neurons would receive input from regions that differentially target LC-GABA neurons (for example, PFC, lateral habenular nucleus, subparafascicular thalamic nucleus, substantia nigra, deep layers of SC, or some regions of the medulla) (Fig. 3f).

Overall, the two types of activity recorded from photo-tagged *Gad2-ChR2* neurons are consistent with the findings of tracing experiments demonstrating similar as well as preferential inputs to

LC-NA and LC-GABA neurons (Fig. 3), and they lead to specific hypotheses about their roles. In one case, regions providing similar inputs may drive both LC-GABA and LC-NA neurons leading to correlated activity in these neurons, and inhibition could act as a feedforward gain control mechanism for arousal (similar to that seen in the cortex with thalamic inputs[34,35]). In the other case, LC-GABA neurons that are broadly anticorrelated to arousal may be driven by a different input source than LC-NA neurons, allowing for independent positive and negative control of arousal.

Coincident inputs to LC-GABA neurons provide gain control of LC-NA neurons. Our anatomical and electrophysiological results imply that a subset of LC-GABA neurons receives coincident inputs with LC-NA neurons. This suggests that feedforward inhibition is present at the level of LC and that local GABA neurons provide gain control to LC-NA neurons. We assessed this hypothesis by presenting auditory tone pips that varied randomly in frequency and amplitude. Tone pips activate LC neurons[15,18,19], potentially by direct inputs from the inferior colliculus, the reticular formation of the pons, and the gigantocellular nucleus of the medulla; all of these regions provide similar magnitudes of input to LC-NA and LC-GABA neurons, as revealed by our anatomical tracer experiments (Fig. 3d–f). Recordings from GCaMP6s-expressing NA axons in the cortex confirmed that LC-NA neurons respond to tone pips (Supplementary Fig. 8a,b). Unit recordings of *Dbh*- and *Gad2-ChR2* neurons (Fig. 6a,b) showed that both responded to tone pips (Fig. 6c). The delay of peak response from the onset of tone pip was 80 ± 14 ms and 51 ± 14 ms for the recorded population of *Dbh* and *Gad2* units, respectively (*n* = 14 and 7 tone-responsive units, *P* = 0.2,
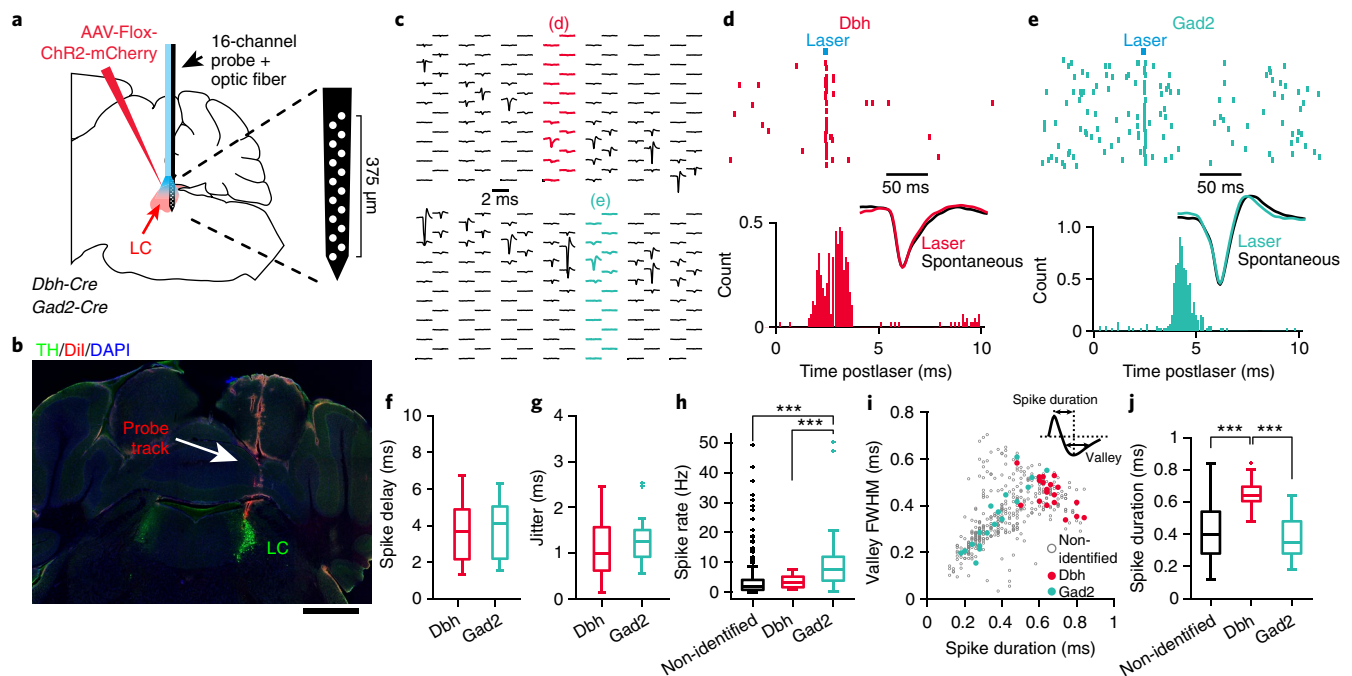
Fig. 4 | Extracellular spike recordings in LC of identified NA and GABA units. a, Methods for photo-tagging *Dbh*- or *Gad2*-ChR2 units using a 16-channel silicone probe equipped with a 100-μm optic fiber. **b**, Probe track (DiI coating) verified with immunohistochemistry staining for TH to identify LC. Scale bar represents 1 mm. **c**, Examples of isolated units and their respective probe locations during two sessions (top, *Dbh*-ChR2; bottom, *Gad2*-ChR2). **d**,**e**, Top, spike rasters from two units responding to 5-ms laser pulses recorded in *Dbh*-ChR2- (**d**) or *Gad2*-ChR2-expressing (**e**) mice. Bottom, distribution of delay from laser onset. Inset, comparison of spontaneous versus laser-evoked spike waveforms. **f**,**g**, Average spike delay and jitter following light activation of *Dbh*-ChR2 and *Gad2*-ChR2 neurons. $P = 0.763$ ($t_{35} = -0.304$) for **f**, and $P = 0.379$ ($t_{35} = -0.8909$) for **g** using two-tailed unpaired *t* test. **h**, Comparison of spontaneous spike rate for all three types of units (one-way ANOVA, $F_{2,430} = 15.88$, $P = 10^{-7}$ using Tukey post hoc test). **i**, Scatter plot of spike duration and valley FWHM values (see inset for definition) for non-identified, *Dbh*-, and *Gad2*-ChR2 units. **j**, Comparison of spike duration for all three types of units (one-way ANOVA, $F_{2,430} = 19.57$, $P = 10^{-9}$ using Tukey post hoc test). $n = 19$, 18, and 396 *Dbh*-ChR2, *Gad2*-ChR2, and non-identified units from 13 mice. Box plots indicate the median (center line), first quartiles (box edges), minimum/maximum values (whiskers), and outliers (+).

two-tailed unpaired *t* test, $t_{19} = 1.3272$). These data suggest that auditory stimuli principally activate coincident inputs to LC-GABA and LC-NA neurons.

Given that tone pips evoked responses in both types of LC neurons, we used these stimuli to assess the possible modulation of LC-NA responses by LC-GABA neurons. We presented a random and sparse sequence of auditory stimuli of different frequencies and intensities to a group of mice, whereas recording pupil diameter (Fig. 6d). Simultaneous recording of pupil diameter and LC-NA activity showed that increase in pupil size followed the increase in LC-NA activity to auditory stimuli (Supplementary Fig. 8b). Silencing NA neurons prevented this pupil dilation response (Supplementary Fig. 8c,d), demonstrating that pupil size can be used to track NA activation with these stimuli. The pupil dilation response to auditory stimuli increased with the intensity of auditory tone independent of tone frequency (Fig. 6e,f and Supplementary Fig. 9a–c). Then, we used *Gad2-Cre* mice injected in the LC with flox-ChR2, with implanted optic fiber, to examine the role of LC-GABA activity on LC-NA responses involving coincident inputs. The trial-averaged traces with or without laser activation demonstrated that activating LC-GABA neurons produced a constricting effect on pupil size, while mild pupil dilation was still detectable after the tone presentation (Fig. 6g). Similar to activating LC-GABA neurons during spontaneous fluctuations of arousal (Fig. 2g,j), we observed a uniform sustained (spanning several seconds) reduction of pupil size across all sound intensities (Fig. 6g–j). To examine the effect of activating LC-GABA neurons on the transient response of LC-NA neurons to sensory stimuli, we removed the tonic effect of LC-GABA activation. We normalized the response for each tone to a 0.5-s baseline

period preceding the tone onset when the laser was already on, and averaged the pupil response for 1.5 s after tone pips (Fig. 6k and Supplementary Fig. 9a). Doing so, we observed that increasing the activity of LC-GABA neurons had a divisive effect on the tone intensity–pupil dilation relationship, as seen by a reduction of slope (or gain) of the pupil size change versus stimulus intensity line (Fig. 6l). This led to enhanced normalized suppression during presentation of tones of higher intensities independent of tone frequency (Fig. 6m,n and Supplementary Fig. 9d), similar to other examples of coincident feedforward inhibition[34,35]. We also tested the effect of activating LC-GABA neurons on the pupil gain response in *VGAT-ChR2* transgenic mice and obtained similar results (Supplementary Fig. 10). Altogether, these results demonstrate that activating LC-GABA neurons alone sets the baseline tone of pupil size, and that coincident activation regulates the gain of LC-NA-mediated arousal.

Non-coincident inputs to LC-GABA neurons non-specifically suppress LC-NA neurons. The results from our retrograde labeling experiments suggest that, along with similar, coincident activation of LC-NA and LC-GABA neurons, some input regions also provide preferential, potentially non-coincident, drive to LC-GABA neurons. Moreover, our electrophysiological data showed that LC-GABA neurons displayed two types of activity, where the activity of Gad2+ (and FS+) neurons was correlated with LC-NA neurons while the activity of Gad2− (and FS−) neurons was broadly anticorrelated with LC-NA activity. We thus wished to examine whether activation of non-coincident inputs to LC-GABA neurons would non-specifically suppress LC-NA activity, and hence regulate arousal tone.

We chose to target inputs from the PFC, as our anatomical data supported the existence of a preferential drive to LC-GABA neurons originating from this region (Fig. 3d–f and Supplementary Fig. 11a). We injected a virus expressing ChR2-mCherry, under the CaMKII promoter to target excitatory neurons, in the orbitofrontal part of the PFC and implanted an optic fiber above the LC to activate PFC axons (Fig. 7a and Supplementary Fig. 11b). Coronal sections of the LC demonstrated the existence of PFC axons in the LC, confirming our results with monosynaptic retrograde labeling (Fig. 7b,c). Most of the PFC axons projected to the anterior and medial part of the LC, where the density of GABA neurons peaks (Figs. 1e and 7c). We activated PFC axons to the LC and indeed recorded significant sustained pupil constriction (lasting several seconds) following laser activation (Fig. 7d). This constriction of pupil size was independent of tone intensity (Fig. 7e–g). Along with activating non-coincident inputs by PFC axonal activation, we activated coincident inputs to LC-NA and LC-GABA neurons with randomly varying auditory tone pips and recorded a transient increase in pupil dilation (Fig. 7h). However, analyzing the tone-induced pupil dilation with and without laser activation revealed no effect of PFC activation on the gain of the transient pupil response (Fig. 7i–k). In contrast to the divisive effect of LC-GABA activation on pupil responses (Fig. 6m), the major effect of PFC activation was a nonspecific reduction in pupil size (Fig. 7g), and hence a net decrease in arousal. These results demonstrate that non-coincident inputs such as from the PFC control the level or tone of LC-NA-mediated arousal, but not the gain, via their preferential targeting of LC-GABA neurons.

Discussion

We demonstrate anatomically and functionally the existence of a local population of GABA neurons in the LC, which inhibits NA activity and thus controls arousal level in the brain, as reflected in pupil size. The pattern of LC afferents is mostly coincident to LC-NA and LC-GABA neurons (Fig. 7l), as shown by tracing experiments and correlated neuronal activity among the two subpopulations. This input pattern supports a role for local LC inhibition in controlling the gain of LC responses. On the other hand, some functionally distinct input regions exert stronger influence on one LC subpopulation over the other, suggesting that the general NA tone

and accompanying arousal level can be set by these inputs (Fig. 7l). An example of this second projection type is the PFC, which projects preferentially to the LC-GABA subregion and alters the tone of NA activity without altering its response gain.

Coincident and non-coincident inputs to LC-GABA neurons affect LC-NA modes of activity on many levels. By regulating the response gain of NA activity to novel stimuli, coincident inputs enable phasic LC activity to be maintained in a certain range, potentially restricting NA activity to an optimal level required for

Fig. 5 | Identified LC-GABA units display two types of activity with respect to pupil size. a, Examples of simultaneous recordings of pupil size and photo-tagged *Dbh*- (upper panel) or *Gad2-ChR2* (middle and lower panels) LC units. Note that the *Gad2* unit in the middle panel is positively correlated (Gad2+), whereas that in the lower panel is negatively correlated with pupil size (Gad2−). **b**, Cumulative probability distribution of the Pearson correlation coefficient of LC unit spike rate with pupil size for all units. The gray area marks non-significant correlations, $P < 0.05$. $n = 19$, 18, and 396 *Dbh-ChR2*, *Gad2-ChR2*, and non-identified units from 13 mice. NS, not significant. **c**, Percentages of *Dbh*- and *Gad2-ChR2* units that are positively or negatively correlated with pupil size. Proportions were significantly different for the two groups (19 of 19 versus 11 of 18 in the *Dbh* and *Gad2* groups; χ^2: 9.11; $P = 0.0025$). The gray portion indicates non-significant correlations, $P < 0.05$. **d**, Average spike rates for different types of units during periods of constricted versus dilated pupil. Each line represents a single unit. Two-tailed paired *t* test: ***$P = 0.0005$ ($t_{18} = 5.36$) for *Dbh*; **$P = 0.0014$ ($t_{10} = 4.38$) for Gad2+; *$P = 0.0208$ ($t_5 = −3.33$) for Gad2−.
e,**f**, Normalized cross-correlation and delay of pupil size to LC firing activity for the classes of units sorted in **b** and **c**. One-way ANOVA, $F_{2,33} = 6.33$, **$P = 0.0088$ using Tukey post hoc test. Box plots indicate the median (center line), first quartiles (box edges), minimum/maximum values (whiskers), and outliers (+). Error bars in **d** and **e** indicate the s.e.m. In **d–f**, $n = 19$, 11, and 6 *Dbh*, Gad2+, and Gad2− units taken from 13 mice.
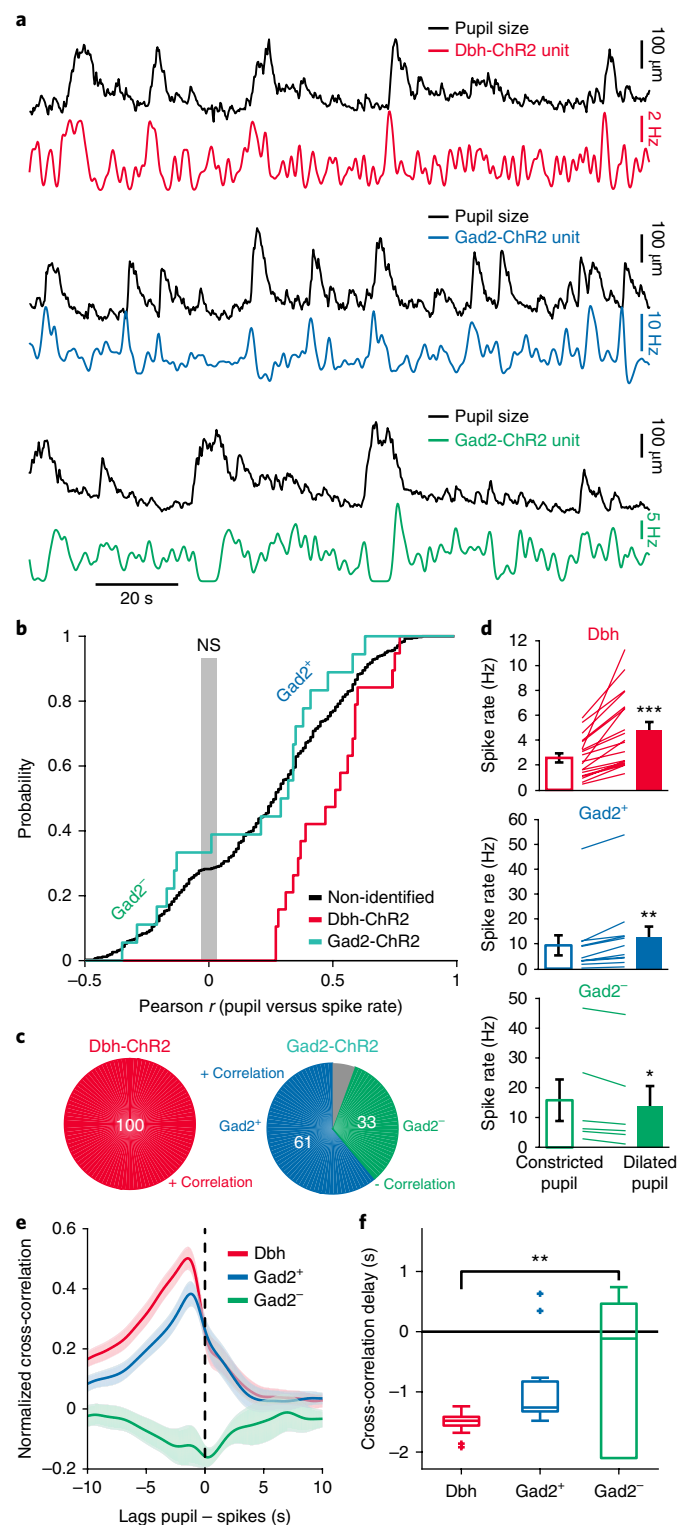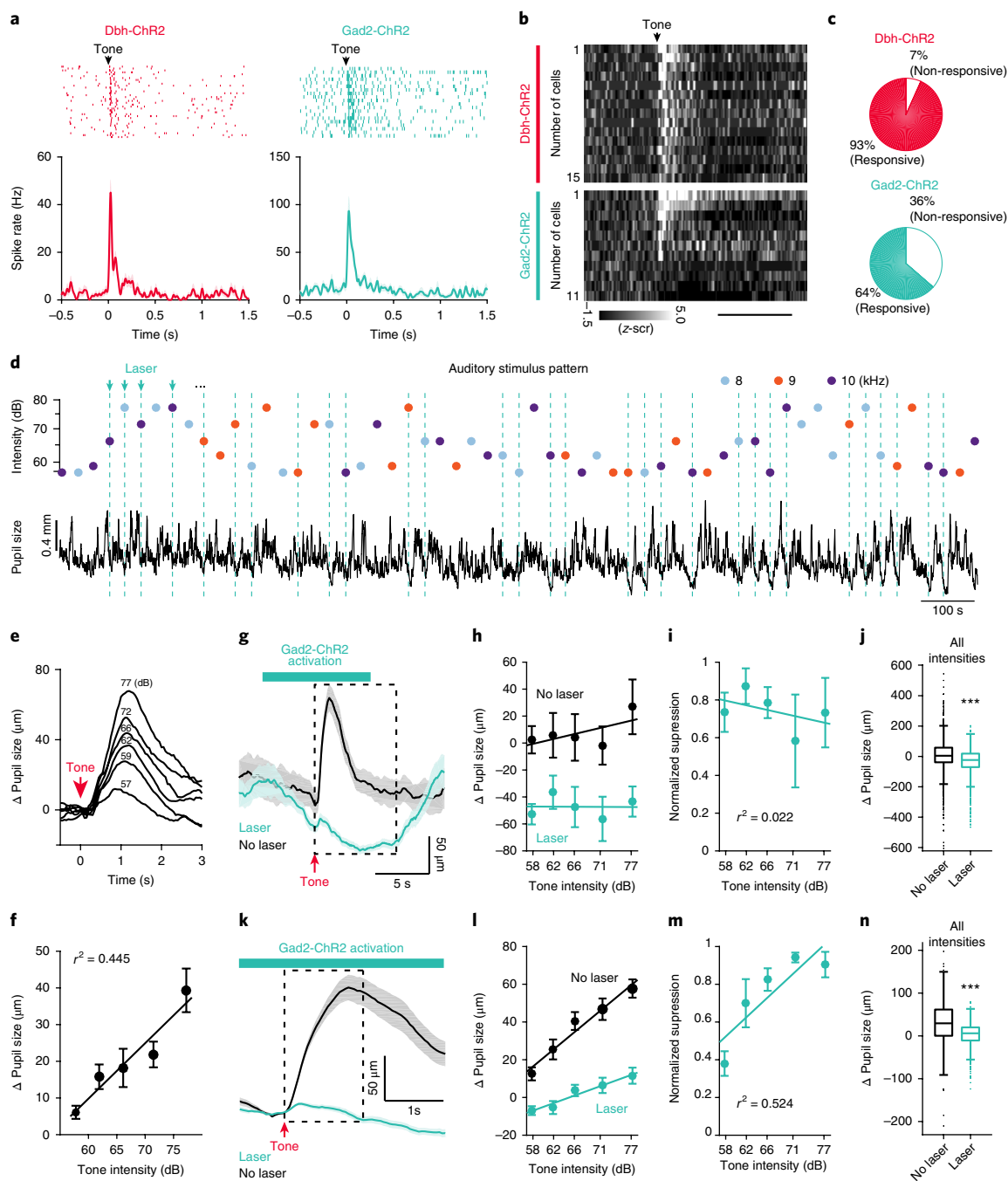
Fig. 6 | LC-GABA neurons control the gain of LC-NA-mediated pupil responses. a, Tone pips presented during the recording of LC photo-tagged units in *Dbh*- (left) and *Gad2*-ChR2-expressing (right) units. Top panels, spike raster plot aligned to tone onset. Bottom panels, session spike rate average. **b**, Raster plots of average responses to tone pips sorted between *Dbh* and *Gad2* units. $n = 15$ and 11 *Dbh* and *Gad2* units, respectively. Scale bar represents 1s. **c**, Percentage of responsive neurons for the two types of units. Proportions were not significantly different for the two groups (14 of 15 versus 7 of 11 in the *Dbh* and *Gad2* groups; χ^2: 3.60; $P = 0.058$). **d**, Top, example of an auditory stimulus pattern used to test the effect of LC-GABA activation on LC-NA responses. Bottom, corresponding pupil size measurement. **e**, Average of pupil size response to tones of different intensities for an example mouse. Each trace is an average of 32–70 trials depending on intensities. **f**, Change in pupil response amplitude with tone intensity (data for $N = 8$ mice recorded in the normal condition, without laser activation. $P = 0.00008$, one-way ANOVA: $F_{4,35} = 8.27$). **g**, Average traces for 77-dB tones with and without laser activation of LC-GABA neurons for one mouse. The dashed box delineates the averaging window used in **h**–**j**. **h**, Pupil size at different tone intensities, with and without laser activation, for the example mouse in **g**. **i**, Normalized suppression of tonic pupil response due to activation of LC-GABA neurons ($P = 0.763$ using one-way ANOVA, $F_{4,15} = 0.46$). **j**, Comparison of laser to no laser trials for all trials regardless of tone intensity or frequency (***$P = 10^{-29}$ using two-tailed unpaired t test, $t_{2973} = 11.37$). **k**, Average traces for the same mouse and condition as in **g**, showing the phasic post-tone-onset response. The dashed box delineates the averaging window used in **l**–**n**. **l**, Pupil size at different tone intensities, with and without laser activation. **m**, Normalized suppression of phasic pupil response to tone intensity due to activation of LC-GABA neurons ($P = 0.00075$ using one-way ANOVA, $F_{4,15} = 8.75$). **n**, Comparison of laser to no laser trials for all trials regardless of tone intensity or frequency (***$P = 10^{-89}$ using two-tailed unpaired t test, $t_{2973} = 20.7995$). For panels **j** and **n**, box plots indicate the median (center line), first quartiles (box edges), minimum/maximum values (whiskers), and outliers (+); $n = 1,494$ and 1,481 laser-off and laser-on trials, respectively. For all other panels, data are displayed as mean ± s.e.m. $N = 4$ mice in **i**, **j**, **m**, and **n**.
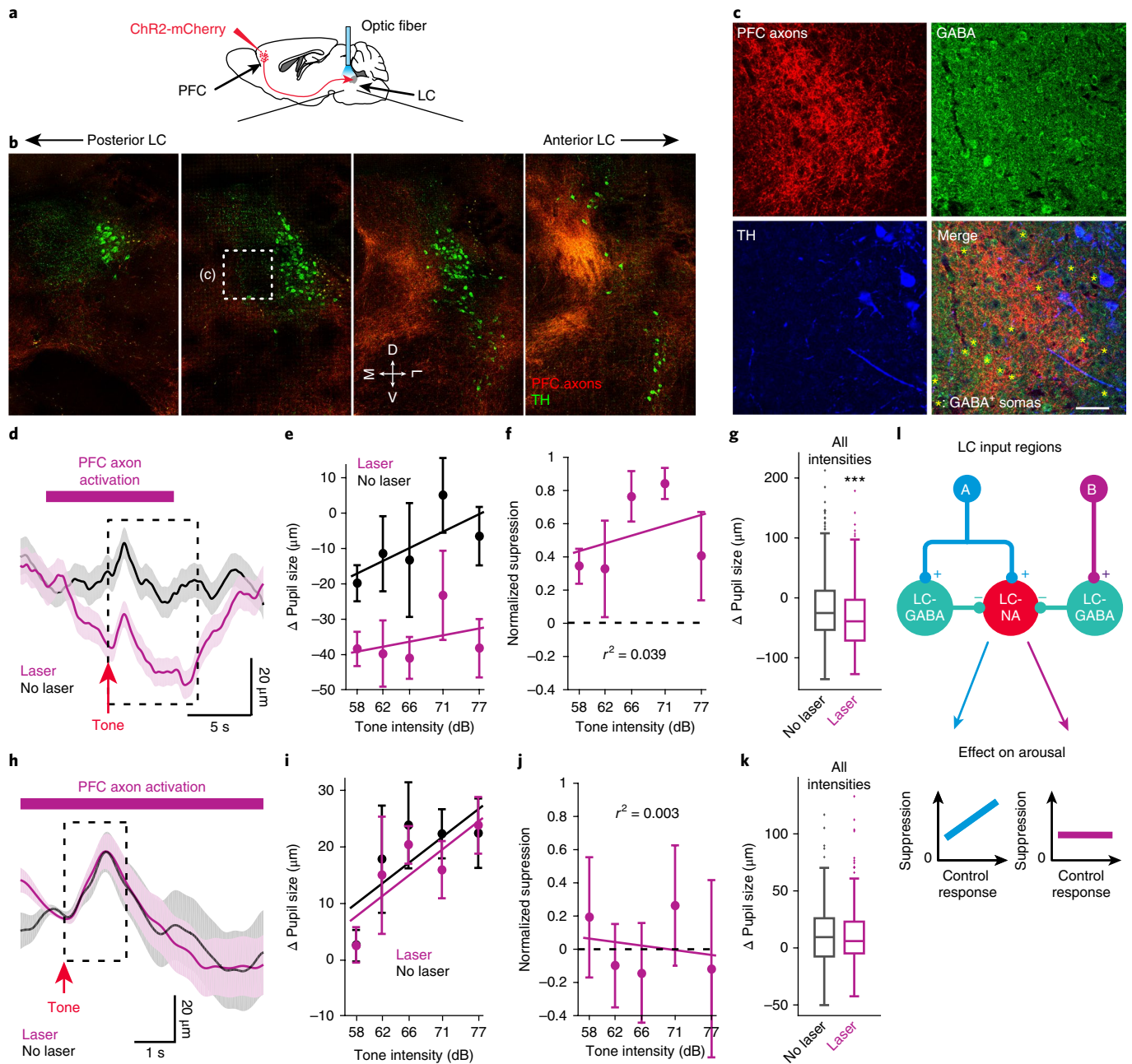
Fig. 7 | Projections from PFC to LC-GABA neurons control LC-NA-mediated pupil tone. a, Methodology used to target PFC projections to LC. **b**, Coronal sections from posterior to anterior LC showing PFC axons in LC and TH staining. Scale bar represents 200 μm. **c**, Confocal images of the region highlighted in **b**. Asterisks indicate GABA⁺ somas. Scale bar represents 50 μm. Experiments in **b** and **c** were repeated in three mice with similar results. **d**, Pupil size in response to tone pips with or without PFC axon activation. Average of all trials for one mouse. The dashed box delineates the averaging window used in **e**–**g**. **e**, Pupil size at different tone intensities, with and without laser activation, for the example mouse in **d**. **f**, Normalized suppression of pupil response as a result of activation of PFC axons in LC ($P = 0.3921$ using one-way ANOVA, $F_{4,10} = 1.14$). **g**, Comparison of laser to no laser trials for all trials regardless of tone intensity or frequency (***$P = 0.00004$ using two-tailed unpaired t test, $t_{577} = 4.14$). **h**, Average traces for the same mouse and condition as in **d**, showing the phasic post-tone onset response. The dashed box delineates the averaging window used in **i**–**k**. **i**, Pupil size at different tone intensities, with and without laser activation. **j**, Normalized suppression of phasic pupil response to tone intensity due to activation of LC-GABA neurons ($P = 0.9493$ using one-way ANOVA, $F_{4,10} = 0.17$). **k**, Comparison of laser to no laser trials for all trials regardless of tone intensity or frequency ($P = 0.9315$ using two-tailed unpaired t test, $t_{577} = 0.086$). **l**, Proposed model of interaction between LC inputs and LC-GABA/LC-NA neurons. Excitatory coincident inputs from region A activate both LC-GABA and LC-NA neurons simultaneously. LC-GABA inhibition scales LC-NA activity divisively, thus controlling the gain of response. Non-coincident inputs from region B target LC-GABA neurons, but not LC-NA neurons (as illustrated here), thus regulating overall NA tone without affecting the response gain. For panels **g** and **k**, box plots indicate the median (center line), first quartiles (box edges), minimum/maximum values (whiskers), and outliers (+); $n = 249$ and 280 laser-off and laser-on trials, respectively. For all other panels, data are displayed as mean ± s.e.m. $N = 3$ mice in **f**, **g**, **j**, and **k**.

cognitive processing[12,23]. By preferentially targeting LC-GABA neurons, non-coincident inputs set thresholds for NA activation and enable modulation of tonic LC activity during different contexts. For example, PFC inputs involved in utility assessment can gate incoming sensory signals to convey the presence or absence of novelty via LC responses[1,36]. Non-coincident drive to LC-GABA neurons can

also affect attentional shifts by interfering with the ability of LC-NA neurons to respond to novel sensory stimuli. Indeed, recordings in the LC of behaving mice have shown adaptation of LC responses to novelty[7,20,37] and a switch of their response to different components of fear conditioning behavior[17]. Alterations in inhibition provided by the regions preferentially driving LC-GABA neurons can explain fluctuations in tonic LC activity observed within sessions in animals performing a visual discrimination task[22], or during the sleep-wake cycle[21,38].

Our results show that LC-GABA neurons are an important source of inhibition for LC-NA neurons. However, we do not exclude other types of inhibitory mechanisms controlling LC activity. First, inhibition in the LC can originate from distal sources. Electrical stimulation of pontine and medullary nuclei, such as the prepositus nucleus, pontine reticular nucleus, and gigantocellular reticular nucleus, yields significant reduction in the firing rate of LC neurons[39,40]. However, these studies never confirmed whether inhibition arose from direct inhibitory projection from these nuclei or from disynaptic pathways, such as from the preferential activation of local GABA neurons. In addition, retrograde labeling studies have shown that a significant GABAergic neuronal population from the posterior lateral hypothalamic area and the CeA projects directly to the LC region, but we do not know the function of these projections in vivo[41]. Second, inhibition in the LC can arise from NA-mediated inhibition. A brief period of inhibition following the phasic response of LC neurons to sensory stimuli[15] has been attributed, in part, to NA-mediated collateral inhibition, since blocking alpha-2 NA receptors moderately suppresses it[39,42]. However, other mechanisms, such as feedforward and feedback inhibition from neighboring LC-GABA neurons, could also explain this postactivation inhibition. Finally, inhibition in the LC can originate from presynaptic release modulation. An example of this is κ-opiate receptors that colocalize with glutamate- and corticotropin releasing factor-positive axons in the LC[43]; activation of these receptors reduces the response of LC neurons to sensory stimuli[43].

The effect of PFC activation on LC activity has remained controversial. Pharmacologically silencing the PFC in rats increases LC activity[44], whereas direct activation of the PFC tends to also increase LC activity[44,45]. It has been an open question as to whether the PFC sends direct descending excitatory or inhibitory projections to LC, and whether an inhibitory influence arises from an indirect pathway. Our monosynaptic tracing results (Fig. 3) reconcile these studies, given that both LC-NA and LC-GABA subpopulations receive direct inputs from the PFC, albeit with a significant preference for LC-GABA neurons. In line with the tracing experiments, we found in some animals a brief period of pupil dilation at the onset of laser activation, reflecting direct inputs to LC-NA neurons (Supplementary Fig. 12). However, an extended period of activation of PFC axons in the LC shows a net pupil constriction effect, consistent with a greater influence on LC-GABA than LC-NA neurons.

Early reports using cholera-toxin B retrograde tracing found a limited number of regions that target the LC region[31,32], which were mostly concentrated in the region adjacent to LC (for example, parabrachial nuclei and gigantocellular nucleus), mesencephalic areas (periaqueductal gray and deep mesencephalic nucleus), and some nuclei of the hypothalamus (for example, preoptic nucleus and LH). Notably, these studies found almost no retrogradely labeled neurons in the cortex, CeA, bed nucleus of the stria terminalis, superior colliculus, and cerebellum, as reported by us here and in another recent report using similar techniques to trace afferent projections to LC (which used *Dbh-Cre* mice and Cre-dependent monosynaptic modified rabies virus)[14]. It should be noted that larger injections of cholera-toxin B in the LC yielded similar results to ours[32], showing inputs from the CeA, bed nucleus of the stria terminalis, and from cortical areas. We and others[14] found that inputs also exist from the cerebellum and superior colliculus. These findings are consistent

with the observation that rabies-mediated trans-synaptic tracing reveals direct synaptic connections[14,46], and provides a more sensitive assay of inputs to LC-NA and LC-GABA circuits than what was reported in the literature with earlier tracers.

Our results highlight the causal relationship between LC-NA activity and pupil dilation. The link between neuronal activity in the LC and pupil size had been previously established in different species[1,5,6]; however, previous studies had not shown that specifically activating or silencing LC-NA neurons increases or decreases pupil size, respectively. LC-NA neurons could control pupil dilation by direct inputs to parasympathetic and sympathetic preganglionic neurons[47,48]. Notably, our results demonstrate that LC-GABA neurons have an essential role in regulating LC-NA activity. In addition to maintaining the dynamic range of LC-NA responses via coincident feedforward inhibition, non-coincident inhibition driven by pathways such as from PFC to LC regulates the global tone of LC activity, and can potentially switch the mode of LC activity in a manner that is dependent on the internal state of the brain.

Online content

Any methods, additional references, Nature Research reporting summaries, source data, statements of data availability and associated accession codes are available at https://doi.org/10.1038/s41593-018-0305-z.

References

1. Aston-Jones, G. & Cohen, J. D. An integrative theory of locus coeruleus-norepinephrine function: adaptive gain and optimal performance. *Annu. Rev. Neurosci.* **28**, 403–450 (2005).
2. Sara, S. J. The locus coeruleus and noradrenergic modulation of cognition. *Nat. Rev. Neurosci.* **10**, 211–223 (2009).
3. Sara, S. J. & Bouret, S. Orienting and reorienting: the locus coeruleus mediates cognition through arousal. *Neuron* **76**, 130–141 (2012).
4. Carter, M. E. et al. Tuning arousal with optogenetic modulation of locus coeruleus neurons. *Nat. Neurosci.* **13**, 1526–1533 (2010).
5. Joshi, S., Li, Y., Kalwani, R. M. & Gold, J. I. Relationships between pupil diameter and neuronal activity in the locus coeruleus, colliculi, and cingulate cortex. *Neuron* **89**, 221–234 (2016).
6. Reimer, J. et al. Pupil fluctuations track rapid changes in adrenergic and cholinergic activity in cortex. *Nat. Commun.* **7**, 13289 (2016).
7. Takeuchi, T. et al. Locus coeruleus and dopaminergic consolidation of everyday memory. *Nature* **537**, 357–362 (2016).
8. Tervo, D. G. R. et al. Behavioral variability through stochastic choice and its gating by anterior cingulate cortex. *Cell* **159**, 21–32 (2014).
9. McCall, J. G. et al. CRH engagement of the locus coeruleus noradrenergic system mediates stress-induced anxiety. *Neuron* **87**, 605–620 (2015).
10. Reimer, J. et al. Pupil fluctuations track fast switching of cortical states during quiet wakefulness. *Neuron* **84**, 355–362 (2014).
11. Vinck, M., Batista-Brito, R., Knoblich, U. & Cardin, J. A. Arousal and locomotion make distinct contributions to cortical activity patterns and visual encoding. *Neuron* **86**, 740–754 (2015).
12. McGinley, M. J., David, S. V. & McCormick, D. A. Cortical membrane potential signature of optimal states for sensory signal detection. *Neuron* **87**, 179–192 (2015).
13. Polack, P. O., Friedman, J. & Golshani, P. Cellular mechanisms of brain state-dependent gain modulation in visual cortex. *Nat. Neurosci.* **16**, 1331–1339 (2013).
14. Schwarz, L. A. et al. Viral-genetic tracing of the input-output organization of a central noradrenaline circuit. *Nature* **524**, 88–92 (2015).
15. Aston-Jones, G. & Bloom, F. E. Norepinephrine-containing locus coeruleus neurons in behaving rats exhibit pronounced responses to non-noxious environmental stimuli. *J. Neurosci.* **1**, 887–900 (1981).
16. Martins, A. R. & Froemke, R. C. Coordinated forms of noradrenergic plasticity in the locus coeruleus and primary auditory cortex. *Nat. Neurosci.* **18**, 1483–1492 (2015).
17. Uematsu, A. et al. Modular organization of the brainstem noradrenaline system coordinates opposing learning states. *Nat. Neurosci.* **20**, 1602–1611 (2017).
18. Hervé-Minvielle, A. & Sara, S. J. Rapid habituation of auditory responses of locus coeruleus cells in anaesthetized and awake rats. *Neuroreport* **6**, 1363–1368 (1995).

19. Grant, S. J., Aston-Jones, G. & Redmond, D. E. Jr. Responses of primate locus coeruleus neurons to simple and complex sensory stimuli. *Brain Res. Bull.* **21**, 401–410 (1988).

20. Vankov, A., Hervé-Minvielle, A. & Sara, S. J. Response to novelty and its rapid habituation in locus coeruleus neurons of the freely exploring rat. *Eur. J. Neurosci.* **7**, 1180–1187 (1995).

21. Aston-Jones, G. & Bloom, F. E. Activity of norepinephrine-containing locus coeruleus neurons in behaving rats anticipates fluctuations in the sleep-waking cycle. *J. Neurosci.* **1**, 876–886 (1981).

22. Usher, M., Cohen, J. D., Servan-Schreiber, D., Rajkowski, J. & Aston-Jones, G. The role of locus coeruleus in the regulation of cognitive performance. *Science* **283**, 549–554 (1999).

23. Yerkes, R. M. & Dodson, J. D. The relation of strength of stimulus to rapidity of habit-formation. *J. Comp. Neurol. Psychol.* **18**, 459–482 (1908).

24. Aston-Jones, G., Zhu, Y. & Card, J. P. Numerous GABAergic afferents to locus ceruleus in the pericerulear dendritic zone: possible interneuronal pool. *J. Neurosci.* **24**, 2313–2321 (2004).

25. Jin, X. et al. Identification of a group of GABAergic neurons in the dorsomedial area of the locus coeruleus. *PLoS ONE* **11**, e0146470 (2016).

26. Boucetta, S., Cissé, Y., Mainville, L., Morales, M. & Jones, B. E. Discharge profiles across the sleep-waking cycle of identified cholinergic, GABAergic, and glutamatergic neurons in the pontomesencephalic tegmentum of the rat. *J. Neurosci.* **34**, 4708–4727 (2014).

27. Cox, J., Pinto, L. & Dan, Y. Calcium imaging of sleep-wake related neuronal activity in the dorsal pons. *Nat. Commun.* **7**, 10763 (2016).

28. Xu, Y. L. et al. Neuropeptide S: a neuropeptide promoting arousal and anxiolytic-like effects. *Neuron* **43**, 487–497 (2004).

29. Zhao, S. et al. Cell type–specific channelrhodopsin-2 transgenic mice for optogenetic dissection of neural circuitry function. *Nat. Methods* **8**, 745–752 (2011).

30. Wickersham, I. R., Sullivan, H. A. & Seung, H. S. Production of glycoprotein-deleted rabies viruses for monosynaptic tracing and high-level gene expression in neurons. *Nat. Protoc.* **5**, 595–606 (2010).

31. Aston-Jones, G. et al. in *Progress in Brain Research* (eds Barnes, C. D. & Pompeiano, O.) Ch. 4 (Elsevier, Amsterdam, Netherlands, 1991).

32. Luppi, P. H., Aston-Jones, G., Akaoka, H., Chouvet, G. & Jouvet, M. Afferent projections to the rat locus coeruleus demonstrated by retrograde and anterograde tracing with cholera-toxin B subunit and *Phaseolus vulgaris* leucoagglutinin. *Neuroscience* **65**, 119–160 (1995).

33. Totah, N. K., Neves, R. M., Panzeri, S., Logothetis, N. K. & Eschenko, O. The locus coeruleus is a complex and differentiated neuromodulatory system. *Neuron* **99**, 1055–1068.e6 (2018).

34. Wilson, N. R., Runyan, C. A., Wang, F. L. & Sur, M. Division and subtraction by distinct cortical inhibitory networks in vivo. *Nature* **488**, 343–348 (2012).

35. Atallah, B. V., Bruns, W., Carandini, M. & Scanziani, M. Parvalbumin-expressing interneurons linearly transform cortical responses to visual stimuli. *Neuron* **73**, 159–170 (2012).

36. Stalnaker, T. A., Cooch, N. K. & Schoenbaum, G. What the orbitofrontal cortex does not do. *Nat. Neurosci.* **18**, 620–627 (2015).

37. Bouret, S. & Sara, S. J. Reward expectation, orientation of attention and locus coeruleus-medial frontal cortex interplay during learning. *Eur. J. Neurosci.* **20**, 791–802 (2004).

38. Nitz, D. & Siegel, J. M. GABA release in the locus coeruleus as a function of sleep/wake state. *Neuroscience* **78**, 795–801 (1997).

39. Ennis, M. & Aston-Jones, G. Evidence for self- and neighbor-mediated postactivation inhibition of locus coeruleus neurons. *Brain Res.* **374**, 299–305 (1986).

40. Mileykovskiy, B. Y., Kiyashchenko, L. I., Kodama, T., Lai, Y. Y. & Siegel, J. M. Activation of pontine and medullary motor inhibitory regions reduces discharge in neurons located in the locus coeruleus and the anatomical equivalent of the midbrain locomotor region. *J. Neurosci.* **20**, 8551–8558 (2000).

41. Dimitrov, E. L., Yanagawa, Y. & Usdin, T. B. Forebrain GABAergic projections to locus coeruleus in mouse. *J. Comp. Neurol.* **521**, 2373–2397 (2013).

42. Aghajanian, G. K., Cedarbaum, J. M. & Wang, R. Y. Evidence for norepinephrine-mediated collateral inhibition of locus coeruleus neurons. *Brain Res.* **136**, 570–577 (1977).

43. Kreibich, A. et al. Presynaptic inhibition of diverse afferents to the locus ceruleus by kappa-opiate receptors: a novel mechanism for regulating the central norepinephrine system. *J. Neurosci.* **28**, 6516–6525 (2008).

44. Sara, S. J. & Hervé-Minvielle, A. Inhibitory influence of frontal cortex on locus coeruleus neurons. *Proc. Natl Acad. Sci. USA* **92**, 6032–6036 (1995).

45. Jodo, E., Chiang, C. & Aston-Jones, G. Potent excitatory influence of prefrontal cortex activity on noradrenergic locus coeruleus neurons. *Neuroscience* **83**, 63–79 (1998).

46. Callaway, E. M. & Luo, L. Monosynaptic circuit tracing with glycoprotein-deleted rabies viruses. *J. Neurosci.* **35**, 8979–8985 (2015).

47. Szabadi, E. Modulation of physiological reflexes by pain: role of the locus coeruleus. *Front. Integr. Neurosci.* **6**, 94 (2012).

48. Samuels, E. R. & Szabadi, E. Functional neuroanatomy of the noradrenergic locus coeruleus: its roles in the regulation of arousal and autonomic function part I: principles of functional organisation. *Curr. Neuropharmacol.* **6**, 235–253 (2008).

Acknowledgements

Author contributions

V.B.-P. and M.S. designed the experiments and wrote the manuscript. V.B.-P. carried out the experiments.

Competing interests

The authors declare no competing interests.

Additional information

Supplementary information is available for this paper at https://doi.org/10.1038/s41593-018-0305-z.

Reprints and permissions information is available at www.nature.com/reprints.

Correspondence and requests for materials should be addressed to M.S.

Publisher's note: Springer Nature remains neutral with regard to jurisdictional claims in published maps and institutional affiliations.

Methods

Animals. All procedures were approved by the Massachusetts Institute of Technology's Animal Care and Use Committee and conformed to National Institutes of Health guidelines. Adult mice (>2 months old) from a C57BL/6J background were used in this study. Male or female mice were randomly selected for each experiment. We used the following mouse lines for the specific expression of various viruses in NA, GABAergic, and cholinergic neurons: *TH-Cre* (B6. Cg-Tg(Th-cre)1Tmd/J, Jackson Laboratory), *Dbh-Cre* (B6.FVB(Cg)-Tg(Dbh-cre) KH212Gsat/Mmucd, MMRRC), *Gad2-IRES-Cre* (Gad2tm2(cre)Zjh/J, Jackson Laboratory). Optogenetic activation of LC GABAergic neurons (LC-GABA) was also done on *VGAT-YFP-ChR2* mice (B6.Cg-Tg(Slc32a1-COP4*H134R/ EYFP)8Gfng/J, Jackson Laboratory). Some experiments were carried out on C57Bl/6 wild-type mice.

Stereotactic surgeries. The preparation of animals was similar for all surgical procedures. They were performed under isoflurane anesthesia while maintaining body temperature at 37.5 °C using an animal temperature controller (ATC2000, World Precision Instruments). After deep anesthesia was confirmed, mice were placed in a stereotaxic frame (51725D, Stoelting), scalp hairs were removed with hair-remover cream, the underlying skin was cleaned with 70% alcohol and betadine, and an incision was made in the scalp. The conjunctive tissue was removed by rubbing hydrogen peroxide on the skull. The skull was positioned such that the lambda and bregma marks were aligned on the anteroposterior and dorsoventral axes. For all surgeries, analgesic was given once before and for 3 d following surgery.

For viral injections, a small hole was drilled through the skull at the location of interest. We used the following coordinates (according to bregma, in mm): LC: −5 to −5.2 anteroposterior, ±0.9 mediolateral, and 2.9–3 dorsoventral; orbitofrontal cortex (PFC): 2.6 anteroposterior, ±1.3 mediolateral, and 2.0 dorsoventral. Viruses were delivered with a thin glass pipette at a rate of 100–200 nl min^{-1} by an infuser system (QSI 53311, Stoelting). The following viruses (titer: ~10^{-12} virus molecules per ml) were injected for imaging and optogenetic experiments: Flex-GCaMP6s (AAV1.Syn.Flex.GCaMP6s.WPRE.SV40, Penn Vector Core), Flox-ChR2-mCherry (AAV1.EF1.dflox.hChR2-(H134R).mCherry.WPRE.Hgh, Penn Vector Core), Flex-ArchT-tdTomato (AAV2-CAG-Flex-ArchT-tdTomato, UNC Vector Core), Flex-tdTomato (AAV1-Flex-tdTomato, UNC Vector Core), and (AAV5/CamKIIalpha-hChR2-(H134R)-mCherry-WPRE-pA, UNC Vector Core). We delivered a volume of 400–500 nl per injection site in the LC of *Dbh-Cre*, and in the PFC of wild-type mice. For experiments using *TH-Cre* and *Gad2-Cre* mice, 200-nl injections were done in the LC to avoid infection of other areas. We confirmed that the virus infection was limited to the LC region for *TH-Cre* animals injected with Flex-GCaMP6s, and did not spread to the ventral tegmental area. After injection, the skin was sutured and we let mice recover for 4–6 weeks after injection of virus for optimal opsin or calcium-indicator expression. For rabies monosynaptic tracing experiments, we injected rAAV1/SynP-DIO-sTpEpB helper virus in the LC of *Dbh-Cre*, *Gad2-Cre*, or wild-type mice. Then, 3 weeks after the first virus injection, we injected the EnVA-RΔG.mCherry (400–500 nl) in the same location.

Optic fibers with 200-μm diameter were implanted with the following procedures. After anesthesia and animal preparation, the scalp was removed, the skull was cleared of conjunctive tissue, and the neck muscles were retracted from the interparietal and occipital plates. After careful alignment of the skull, the optic fiber cannula was held by a stereotaxic manipulator and inserted at different locations (see virus injections for coordinates) slightly on top of (~200 μm dorsoventral) the targeted region. Two-ferrule cannulas (TFC_200/245-0.37_ 4mm_TS2.0_FLT, Doric Lenses) were used for LC implantation. A single fiber optic cannula (CFM12L05, Thorlabs) was implanted in LC for activation of LC PFC axons. For LC PFC axon activation, the cannula was implanted using the following coordinates to target the anterior and medial part of LC: −4.5 to −4.8 anteroposterior, ±0.5 mediolateral, and 2.5 dorsoventral. The cannula was attached to the skull with dental cement (Teets Denture Material, or C&B Metabond, Parkell). To avoid light reflection and absorption, dental cement was mixed with black ink pigment (Black Iron Oxide 18727, Schmincke). A custom-designed head plate[49] was also implanted at the end of the surgery for head fixation.

To perform LC single unit recording in awake head-fixed mice, we implanted a head plate 1–2 weeks before recording. We used a custom design stereotactic arm to align the head plate parallel to the median and dorsal line of the skull during implantation. The head plate was attached to the skull using dental cement. The exposed skull was protected using rapid curing silicone elastomer (Kwik-Cast, WPI) topped with a fine layer of dental cement.

Two-photon calcium imaging was done through a cranial window. Following virus injection of GCaMP6s in the LC of *TH-Cre* or *Dbh-Cre* mice, we drilled a 3-mm circular window centered over the anterior part of V1 (~3.5 mm posterior and ~2 mm lateral to bregma) or the medial PFC (~2 mm anterior to bregma and centered on the midline). A 3-mm centered on a 5-mm coverslip (CS-5R and CS-3R, Warner Instruments), and glued together with ultraviolet adhesive (NOA 61 UV adhesive, Norland Products), was positioned over the craniotomy and attached to the skull using dental cement (C&B Metabond, Parkell). A head plate was also attached to the skull for head fixation.

Pupil and body movement monitoring. After fixing the mouse head using a previously implanted head plate, a high-resolution CMOS camera (DCC1545M, Thorlabs) equipped with a 1.0× telecentric lens (58–430, Edmund Optics) was pointed at either the left or right eye depending on the experimental set up. Infrared illumination at 780 nm was provided by a light-emitting diode array light source (LIU780A, Thorlabs). Illumination was done at an angle of ~60° for the corneal reflection spot to be cleared of pupil visualization. Video acquisition of eye images (240 × 184 pixels) was performed at 20 Hz by a custom-made MATLAB script. The ambient illumination was controlled by a 7" monitor (700YV, Xenarc Direct) placed 8 cm in front of the mouse and displayed a full-field gray stimulus at an illuminance of ~57 lx (403125, Extech Instruments). This level of ambient illumination was sufficient to keep the pupil constricted within the space between the two eyelids. In all experiments, a master computer, controlling the visual and auditory stimuli, triggered pupil camera acquisition, as well as two-photon imaging, optogenetic manipulations, or extracellular electrophysiology recordings via various data acquisition cards depending on the experiment (PCI-DIO24, Measurement Computing; NI USB-6259 or BNC-2110, National Instruments). Time stamps of every pupil frame were saved for further alignment with imaging, electrophysiology, or optogenetic experiments.

We segmented the images of a black pupil on a gray iris background by a sequence of image processing manipulations done with a custom-made MATLAB script. We adjusted the minimum and maximum pixel intensity of pupil images. We then normalized pixel values by the convolution of pupil frames by a 5 × 5-pixel kernel matrix of equal values. The images were binarized by a threshold value manually decided for each experiment. The binary images were filtered to extract the largest components located in the center of the image. The isolated binarized pupil image was then fitted with a least square fit of ellipse. From this fit we estimated the diameter of the pupil for each frame. The pupil segmentation was either done online, during the experiments, or offline on saved images of the pupil. Using this pipeline for pupil segmentation, very few frames had to be dropped due to poor fitting of the pupil. Most of the dropped frames were due to eye blinking or excessive micro-saccades and the diameters for these frames were estimated by interpolation.

To monitor body movement, we used a 720p high-definition camera pointed at the mouse (LifeCam Cinema, Microsoft). The sampling rate used was 10 Hz. Movement data were synced with other experiments by displaying an indicator on the monitor. The movement metric was calculated by extracting the pixel data in time for regions around the nose, the neck, the paws, and the ears of the animal. The mean difference in pixel value between each frame was calculated for each region and we normalized this value over a region of the image where no movements were expected. Periods of activity or quietness were isolated using a threshold value of 0.5 s.d. on the movement trace.

Optogenetic modulation of LC. We used solid state laser illumination at 473 and 532 nm for activating ChR2 and ArchT, respectively (MBL-III-473/1~200 mW or MGL-III-532/1~300 mW, Opto Engine). A 200-μm/0.39 numerical aperture patch cable (M72L02, Thorlabs) was connected to the laser output and to an intensity division cube (DMC_1×2i_VIS_FC, Doric Lenses) for bilateral LC modulation. The patch cable (200 μm/0.39 numerical aperture; M83L01 or M81L01, Thorlabs) was attached to the animal ferrule implant using corresponding ceramic mating sleeves. To block any light emitting from the interface between the patch cable and the implanted ferrule, a piece of black electrical tape was wrapped around the connection. The laser pulse duration, frequency, and shape were controlled by a data acquisition system (Digidata 1440A, Molecular Devices) connected directly to the analog port of the laser power supply. For ChR2 activation of NA$^+$, 10-ms pulses at a frequency of 3, 5, 10, or 30 Hz for 0.1, 0.5, 1, and 2 s were applied depending on the experiment. The peak power of every pulse was 4–5 mW at the laser output. For ChR2 activation of LC-GABA neurons, a sine wave at 25 Hz was used for various durations. A small ramp up (duration 0.5 s) and ramp down (duration ~5 s) in power was applied on top of the sine wave. Low-power light stimulation (peak power <3 mW) was used for *VGAT-ChR2-YFP* mice to keep the spread of optical activation in the vicinity of the optic fiber end, thus increasing neuronal activity only in GABA neurons surrounding LC. For direct inactivation of LC-NA$^+$ neurons with ArchT, 15–17 mW of power was applied for 4 s. The rebound effect of inactivation was prevented by ramping down the laser power at the end of each laser pulse for 1 s. For activation of PFC axons in the LC, 10-ms pulses at a frequency of 20 Hz were applied for 10 s. The peak power for those experiments ranged from 12 to 18 mW. At the end of each experiment, the location of the optic was verified with respect to neurons expressing the opsin in the brain. For *Gad2-Cre*, *VGAT-ChR2-YFP*, and LC-PFC experiments, location was also verified with respect to LC-NA by immunohistochemistry for TH.

Slice electrophysiology. At 4–6 weeks after virus injection of *Flox-ChR2* in the LC of *Gad2-Cre* mice, deeply anesthetized animals (isoflurane) were transcardially perfused with modified ice-cold ACSF containing (in mM): 210.3 sucrose, 2.5 KCl, 1 NaH$_2$PO$_4$, 26 NaHCO$_3$, 7 MgSO$_4$, 0.5 CaCl$_2$, and 11 D-glucose. The posterior brain was then quickly removed, placed in a microtome (Leica VT1200 S), and sliced in the coronal plane at a thickness of 0.3 mm. Slice recovery was performed at 37 °C for 30 min in normal ACSF containing (in mM): 128 NaCl, 2.5 KCl,

1 NaH_2PO_4, 26 $NaHCO_3$, 1.3 $MgSO_4$, 2 $CaCl_2$, and 10 D-glucose. After recovery, slices were maintained at room temperature for the remainder of the experiment in normal artificial cerebrospinal fluid (ACSF). ACSF was bubbled with a mixture of 95% O_2 and 5% CO_2 throughout the entire experiment.

For recording, slices were placed in a chamber perfused with oxygenated ACSF at a rate of 2 ml min^{-1}. To block glutamatergic transmission, 10 μM 6-cyano-7-nitroquinoxaline-2 (CNQX, 1045, Tocris) and 10 μM D-AP5 (0106, Tocris) were added to the bath solution for all recordings. We used a cesium chloride-based intracellular solution for voltage clamp recordings of inhibitory currents (in mM): 135 CsCl, 10 HEPES, 1 EGTA, 4 Mg*ATP, 1 Na_2*GTP, 8 Na_2-phosphocreatine, 3 biocytin; and a K-gluconate-based solution for current clamp recordings (in mM): 135 K-gluconate, 6 KCl, 10 HEPES, 4 Mg*ATP, 0.3 Na_2*GTP, 0.1 EGTA, 8 Na_2-phosphocreatine. Osmolality was set to 290–295 (mOsm) and pH to 7.2. Electrode resistance ranged from 3 to 5 MΩ. To block glycinergic receptors we bath applied 1 μM strychnine (ab120416, Abcam) and to block $GABA_A$ receptors we applied 20 μM bicuculline (0131, Tocris). Light activation was performed by pulsing for 5 ms at 10–15 mW every 2 s a solid-state blue laser (MBL-F-473-300mW, Opto Engine) connected to the light path of our microscope (BX61WI, Olympus; CBH-1.0, Siskiyou). Neurons were visualized through differential interference contrast (DIC) or fluorescence using a charge-coupled device (CCD) camera (ORCA-R[2] C10600, Hamamatsu). *Gad2*-ChR2-positive neurons were targeted by their expression of mCherry fluorophores. LC-NA neurons were identified by fixing the slice overnight with 4% paraformaldehyde and immunohistochemistry against TH (see the Histology section). Recordings were performed with a Multiclamp 700b (Molecular Devices) amplifier, digitized at 10 kHz, and low-pass filtered at 1 kHz with a Digidata 1440 and pClamp10 software (Molecular Devices). We recorded the spontaneous spiking activity of TH^{+} neurons by performing cell-attached recordings for 2 min before opening the cell membrane to achieve whole-cell configuration. Neurons were voltage clamped at a membrane potential of −70 mV to record light-evoked currents. The V_{Cl} reversal potential was 0.10 mV for the CsCl-based solution. To measure the effect of *Gad2*-ChR2 activation on the spike rate of TH-positive neurons, we compared the average spike rate of 50-ms periods taken before light activation and right after the onset of the 5-ms pulse. The amplitude of evoked IPSCs was measured as the peak current after light activation for each condition. Access resistance ranged from 10 to 15 MΩ and recordings with variations greater than 15% of the baseline resistance value were excluded.

Single unit recordings of photo-identified LC units in awake mice. One or two days before the experiments, mice were head-fixed for 1 h to habituate to head fixation. On the day of the experiments, the mice were anesthetized with isoflurane and the dental cement and silicone elastomer on the skull were removed. The mouse was placed on the stereotaxic frame and a 500-μm diameter craniotomy was performed on top of the inferior colliculus (from bregma: −4.9 to −5.4 mm anteroposterior and 0.6–1.1 mm mediolateral). The dura was removed and the craniotomy was protected with saline and a piece of gelfoam (Pfizer). The skull was covered again with silicone and the animal was allowed to recover for at least 2–3 h for the anesthesia effect to washout completely. The awake animal was then head-fixed and the silicone and gelfoam removed gently. A 0.9% NaCl solution was used to keep the surface of the brain wet for the duration of the recordings.

After placing the animal in the recording set up, we submerged a reference silver wire in the NaCl solution on the skull surface. The position of the 16-channel silicone probe was referenced on bregma and the surface of the brain and lowered slowly (1 min per mm) to 2.0 mm in the ventral axis using a motorized micromanipulator (MP-285, Sutter Instrument Company). The extracellular signal was amplified using a 1× gain headstage (model E2a, Plexon) connected to a 50× preamp (PBX-247, Plexon) and digitized at 50 kHz. The signal was high-pass filtered at 300 Hz.

For optical identification (photo-tagging) of LC-NA and LC-GABA units, we used a solid-state blue laser (MBL-III-473/1~200 mW, Opto Engine) connected via a 105-μm/0.22 numerical aperture patch cable (M61L01, Thorlabs) to an optic fiber glued to 16 channel recording probes (A1x16-Poly2-5mm-50s-177-OA16LP, NeuroNexus). Light pulses of 2–5 ms at various light intensities (0.1–15 mW) were then repeatedly delivered in the tissue (frequency: 1 or 2 Hz), and each channel was screened for light-evoked events. Spikes were considered light responsive if they responded within 10 ms after light stimulus onset. We also kept only units responding to at least 75% of laser pulses, and whose light-evoked waveforms closely matched the spontaneous ones. During our recordings, we minimized the power of light excitation to minimize the light-induced artifact. Recording sessions without light-responsive units were excluded from analysis.

For verifying the probe location after recordings, the silicone probe was gently retracted and the recording tract was marked by re-entering the DiI-coated probe (2 mg ml^{-1}; D3911, ThermoFisher) at the same location. The brain was harvested postexperiment and immunohistochemistry for confirming the probe location was performed. Spikes were monitored online with amplitude threshold using Plexon Recorder software, but re-sorted offline using a fully automated spike-sorting algorithm[50]. Spike curation was done manually to remove artifacts picked by the algorithms (ill-shaped spikes) and spikes with low amplitudes or low spontaneous spike rate (<0.1 spikes s^{-1}). We verified spike times with cross-correlograms to eliminate duplicates. We excluded parts of the recordings with obvious drift (units jumping from one channel to another).

Two-photon imaging of LC-NA axons. Four weeks after virus injection, GCaMP6s^{+} NA axons were imaged in the cortex using a Prairie Ultima IV two-photon microscopy system. Mice were head-fixed and a light shield was attached to their head plates, and the 25×/1.05 numerical aperture objective (XLPlan N, Olympus) was lowered on top of their cranial window. The 920-nm excitation of GCaMP6s was provided by a Ti:sapphire tunable laser (Mai-Tai eHP, Spectra-Physics). Power at the objective ranged from 10 to 30 mW depending on GCaMP6s expression levels. After locating axons at 4× optical zoom, their activity was acquired at 5 frames per second for 10-min blocks while simultaneously imaging the pupil using 8× optical zoom. Axons with significant signal-to-noise ratio were selected for analysis. We imaged 3–8 axons per mouse. The majority of our imaging field of view contained only one axon. After recording one field of view, we moved at least 1 mm away to find new axons. Care was taken to select axons from different branches, even though we cannot exclude the possibility that axons we considered arising from different neurons were actually branches arising outside our imaging window. Using these criteria, 31 axons were recorded from 6 mice.

After acquisition, time-lapse imaging sequences were corrected for x and y movement using template-matching ImageJ plugins[51]. Multiple circular region of interests (3–7) were taken along each axon to extract the fluorescence intensity. The intensity in time for each region was then averaged together (F) to minimize the noise in our signal. The $dF/F = (F − F_0)/F_0$ signal was calculated from this average by taking the mode of the signal as the reference value (F_0).

Sound stimuli. Tone pips were delivered using a single speaker (HK195, Harman/Kardon) located at a distance of 30 cm from the mouse. Sound stimuli were created and delivered using Psych-toolbox in MATLAB. Tone sequence was randomized in intensity and frequency to avoid habituation of the response. The interstimulus interval was set at 30 s. Tone intensity was set to 75 dB and 15 s interstimulus interval for electrophysiological recordings. The duration of each stimulus was fixed at 0.5 s. The speaker frequency range was calibrated using a USB calibrated measurement microphone (UMIK-1, Mini DSP) and the Room EQ Wizard software. The ambient noise in the room was estimated around 50 dB and the sound stimulus intensities were recorded by a sound level meter. To obtain the pupil response to different tone intensities and frequencies, an average of 63 ± 5 trials per tone intensity were recorded. To avoid long sessions and habituation, we limited each mouse to one 1-h session per day. For each animal, 5 ± 1 sessions were recorded. For trials with laser activation of LC-GABA neurons in *Gad2*-ChR2, *VGAT-ChR2*, and PFC-LC implanted mice, the laser was turned on 5 s before the auditory tone onset and kept on for a total duration of 10 s (5 s baseline and 5 s after auditory stimulus). Laser activation was applied on 50% of trials distributed randomly during the session. To calculate the effect of laser activation on NA tone, we used a 7-s-long averaging window aligned to sound onset and compared the z-scored laser and non-laser trials. For measuring the modulation of pupil response created by laser activation, a baseline period of 0.5 s before tone onset was used to calculate the increase in pupil size to different tone intensities and the response over a 1.5-s-long averaging window aligned to sound onset was evaluated. Trials with high (2 s.d.) or low (1 s.d.) were excluded from the analysis.

Histology. Under very deep anesthesia, mice were perfused transcardially with 0.9% NaCl followed by 4% PFA. The brains were harvested and postfixed in 4% PFA at 4 °C overnight. In some experiments, brains were extracted without transcardial perfusion and only immersed in PFA overnight. Coronal sections (50 or 100-μm-thick) were cut using a vibratome (VT1200S, Leica) and were incubated overnight at 4 °C in PBS + 0.1% Triton + 3% BSA, and the following primary antibodies were used: 1:1,000 chicken anti-tyrosine hydroxylase (TYH, Aves Labs lot no. TYH8727985), 1:1,000 rabbit anti-VGAT (131002, Synaptic Systems lot no. 131002/34), 1:1,000 rabbit anti-GABA (A2052, Sigma lot no. 126M4791V), 1:500 rabbit anti-neuropeptide S (ab18252 Abcam), and 1:200 streptavidin-488 conjugated antibodies (S32354, ThermoFisher). We used the following secondary antibodies at a dilution of 1:500: goat anti-chicken 647 nm (A21449, ThermoFisher), goat anti-chicken 488 nm (A11039, ThermoFisher), goat anti-rabbit 488 nm (A11034, ThermoFisher), and goat anti-mouse 488 nm (A21121, ThermoFisher). For acute slices from whole-cell electrophysiological recordings, after fixing overnight in 4% PFA, slices were washed 3 × 10 min in PBS and permeabilized with 1% Triton + 3% BSA before incubation with primary antibodies. For GAD67 staining, slices were permeabilized for 1 h in 3% BSA and 10% normal goat serum, and then incubated for 48 h at room temperature in 3% BSA, 10% normal goat serum, and 1:200 mouse anti-GAD67 (MAB5406, EMD Millipore lot no. 2923238). (Note that no detergent was used at any steps for the staining.) Slices were mounted in Vectashield hard set mounting medium with 4,6-diamidino-2-phenylindole (DAPI) (H-1500, Vector Laboratories). The resulting immunofluorescence was imaged with a confocal system (TCS SP8, Leica) with 10×/0.40 numerical aperture, 20×/0.75 numerical aperture, or 63× /1.40 numerical aperture objectives (Leica).

For quantification of *Gad2-Cre* neurons coexpressing GABA, GAD67, TH, and neuropeptide S, 20× z-stack images were acquired for 2–3 fields of view surrounding the LC of each slice. The percentage of *Gad2-Cre* cells, as identified by their expression of Flox-mCherry, overlapping with the different markers was calculated for each field of view. For the reconstruction of LC structures and

surrounding areas, we collected the brain from Flex-tdTomato virus-injected *Dbh-Cre* mice. We performed staining of GABA by immunohistochemistry on the slices covering a region of 1–1.5 mm on the anteroposterior axis that covered the full extent of the LC. The GABA$^+$ and *Dbh*$^+$ neurons of the LC were imaged by performing tiling reconstruction with a 20× objective zoomed 2×. We also took low-magnification (10×) images of each slice for later registration across the different slices. The location of GABA neurons located within 200 μm of *Dbh*$^+$ somas was then marked using ImageJ, and the whole LC was three-dimensionally reconstructed by exporting those values in a custom-made MATLAB program. Due to the different penetration properties of antibodies, quantification was performed within 10 μm of the surface of the slice. All slices were aligned with respect to the center of mass of LC-*Dbh* neurons. To obtain the neuronal density of each LC-NA and LC-GABA neuron, we counted the number of somas in each bin (bin size: 50 or 100 μm) and normalized to the total number of somas counted.

For analysis of inputs to LC-NA versus LC-GABA populations, we collected the brain 1 week after injection of EnVA-RΔG.mCherry. Coronal sections 100 μm thick were produced, and one section every 200 μm was serially mounted on microscope slides. We analyzed sections from the middle of the olfactory bulb (+4.5 mm from bregma) to the end of the brain stem (−8 mm posterior to bregma). Somas positive for mCherry were counted from all selected slices except for regions surrounding LC. The Paxinos and Franklin[52] mouse atlas was used as a reference for identifying brain regions. We also verified our data against the Allen Mouse Brain Atlas[53] and found similar results. Regions adjacent to LC were not considered for analysis due to non-specific expression of virus at the site of injection. The fraction of total inputs for each animal was obtained by dividing the number of mCherry$^+$ soma for each brain region by the total number of somas counted. Animals with too few presynaptic neurons were not considered for analysis. The injection of the same combination of Cre-dependent helper virus and deleted glycoprotein in the LC of 2 wild-type mice showed a small number of neurons positive for mCherry at the injection site, but almost no neurons retrogradely labeled ($n = 9$ and 14 compared with 240 ± 99 and 1767 ± 733 neurons in the *Dbh*- and *Gad2-Cre* conditions), confirming that retrogradely labeled neurons were targeted to Cre-expressing starter cells.

Data processing. All data analysis, unless noted, was performed using custom-made MATLAB scripts.

In single unit recordings, we extracted two classes of unit (regular spiking and FS) based on their waveform shape. For each unit, we calculated the full width at half maximum (FWHM) of the valley portions of the average spike and the spike duration defined by the time from peak to valley. A Gaussian mixture distribution model with three components was fitted to the data. The three clusters were then classified as FS for short spike duration or regular spiking for long spike duration and the third cluster for non-classified units. Valley FWHM and spike duration were used due to the best possible dissociation between FS and regular-spiking units. Spike delay to laser activation for photo-tagged *Gad2* and *Dbh* units was calculated as the average timing for the first peak after the light onset. The jitter was defined as the standard deviation of this peak onset distribution. We calculated the spontaneous firing rate by averaging the number of spikes during a 10-min period, where no sensory stimulus was presented. Instantaneous spiking rate ($r(t)$) was obtained by using a kernel density estimation[54] using the following equations:

$$r(t) = \sum_{i=1}^{N} f_\Delta(t - t_i)$$

where t_i is the time if the ith spike and N is the total number of spikes. f_Δ represents the following exponential kernel:

$$f_\Delta(t) = \frac{1}{\sqrt{2\Delta}} \exp\left(-\sqrt{2} \left| \frac{t}{\Delta} \right|\right)$$

Different methods were employed to evaluate how neuronal or behavioral activity correlate with arousal. For measuring the general association between LC single unit activity and pupil size, we first obtained an estimation of the instantaneous spike rate sampled at 5 Hz. We then computed Pearson's linear correlation coefficient between the pupil size and activity of LC. The value of Pearson's correlation was done at a lag between pupil and neuronal activity corresponding to the peak in cross-correlation. P values for Pearson's correlation were calculated using a Student's t-distribution for a transformation of the correlation. An LC unit correlated significantly with pupil size if $P < 0.05$. The activity of different classes of units during global pupil constriction or dilation was measured by averaging the spike rate during pupil values lower than the 25th percentile (for constriction) or higher than the 75th percentile (for dilation). To measure the timing of correlation with pupil size, we computed the normalized cross-correlation. Pupil traces and neuronal or behavioral activity metrics were resampled (for extracellular LC recordings: 200 Hz, LC-NA Ca^{2+} axonal imaging: 5 Hz, and for facial movements video analyses: 10 Hz) and both normalized using z-score before computing cross-correlation. The delay between arousal and NA activity or movement was derived from the average lag value at maximum cross-correlation. To evaluate the increase in activity preceding pupil dilation or constriction, we band-pass filtered the pupil trace between 0.1 and 2 Hz using a second-order Butterworth filter. We then isolated pupil events by locating either

the time point of minimas (dilation event) or maximas (constriction event) and extracted the pupil and spike rate traces for a window of −1 to 4 s around those time points. The amplitude of spike rate was evaluated from 0 to 0.5 s after the onset of dilation or constriction. Alternatively, we also aligned NA activity (spike rate and calcium imaging) to maximas or minimas of the derivative of pupil size (variation of pupil diameter in time).

The effect of activating diverse populations of the LC on arousal was assessed by measuring the alteration in pupil size following light activation or inactivation of neurons expressing ChR2 or ArchT. For each trial, we subtracted the baseline pupil diameter, evaluated for each trial on a period of 2 s before light onset. We then calculated the change in pupil size by averaging for a period of 1.5–8 s following the onset of the stimulus (*Dbh-ChR2*: 1.5–2 s depending on stimulus duration, *Dbh-ArchT*: 4 s, and *VGAT-ChR2*: 8 s). Since there is a delay between increase or decrease in LC-NA activity and pupil dilation, we averaged the response of optical activation 0.7 s after switching on the laser. The average variation in pupil size was then calculated for each animal. We used trials without laser as control to compensate for spontaneous changes in pupil size.

To evaluate how LC-NA and LC-GABA neurons respond to salient sensory stimuli, we recorded the response of units to tone pips. A unit was considered auditory responsive if there was a significant increase ($P < 0.05$ using one-tailed paired t-test) of activity between a baseline period of 500 ms and the amplitude calculated over a 500-ms period following the onset of tone pip. To evaluate the delay between neuronal response and stimulus onset, we calculated the average time for the response to reach a value above half the standard deviation. For two-photon imaging of LC-NA GCaMP6s$^+$ axon, we compared the response with a 2-s baseline period preceding the auditory stimulus onset.

The effect of LC-GABA neurons on LC-NA-mediated increase in arousal was assessed by recording the pupil diameter while animals were presented auditory stimuli of different intensities. LC-GABA neurons were optically activated by a 25-Hz sine wave (max power ~3 mW) in half of the trials and the order of trials was randomized. Pupil response was calculated by subtracting a baseline pupil size value for each trial before the auditory stimulus (calculated over 0.5 s before tone onset). Since the effect of auditory stimulus on pupil dilation is usually delayed by a few milliseconds, we calculated the average amplitude of pupil for a 1.5-s window 0.5 s after the tone onset. This response was then averaged for each trial type to obtain the tone intensity–pupil size increase relationship. The suppression by LC-GABA neuron activation was defined as the difference between the response for trials with and without light activation. This difference was then normalized to the maximum value of suppression for each animal. The same procedure was used for the optical inactivation of LC-NA neurons with ArchT during sound stimulation. Optical silencing was performed for a total of 4 s (1 s baseline and 3 s poststimulus) and amplitude of pupil size was calculated for 1.4 and 1.6 s, respectively, surrounding the stimulus.

Statistics. Throughout the paper we used paired and unpaired Student's two-sided t-test for evaluating P values of experiments with two conditions. P values for experiments with multiple conditions were computed using analysis of variance (ANOVA) with Tukey post-hoc test. Significance level were marked as *$P < 0.05$, **$P < 0.01$, and ***$P < 0.001$. P values for Pearson's correlation were calculated using a Student's t-distribution for a transformation of the correlation. LC unit correlated significantly with pupil size if $P < 0.05$. Proportions of cells positively or negatively correlated with pupil for *Dbh* and *Gad2* units were tested for significance using a chi-squared (χ^2) test. For all experiments, sample sizes were predetermined using a power analysis to provide at least 80% power to detect an effect. Data distribution was assumed to be normal but this was not formally tested. Data collection and analysis were not performed blind to the conditions of the experiments.

Data availability

The data and code used for analyses that support the findings of this study are available from the corresponding author upon reasonable request.

References

49. Goard, M. J., Pho, G. N., Woodson, J. & Sur, M. Distinct roles of visual, parietal, and frontal motor cortices in memory-guided sensorimotor decisions. *eLife* **5**, e13764 (2016).
50. Chung, J. E. et al. A fully automated approach to spike sorting. *Neuron* **95**, 1381–1394.e6 (2017).
51. Schneider, C. A., Rasband, W. S. & Eliceiri, K. W. NIH Image to ImageJ: 25 years of image analysis. *Nat. Methods* **9**, 671–675 (2012).
52. Paxinos, G. & Franklin, K. B. J. *The Mouse Brain in Stereotaxic Coordinates*. (Academic Press, San Diego, 2001).
53. Lein, E. S. et al. Genome-wide atlas of gene expression in the adult mouse brain. *Nature* **445**, 168–176 (2007).
54. Shinomoto, S. in *Analysis of Parallel Spike Trains* (eds Grün, S. & Rotter, S.) Ch. 2 (Springer US, Boston, 2010).

nature research

Corresponding author(s):   Mriganka Sur

Reporting Summary

Nature Research wishes to improve the reproducibility of the work that we publish. This form provides structure for consistency and transparency in reporting. For further information on Nature Research policies, see <u>Authors & Referees</u> and the <u>Editorial Policy Checklist</u>.

Statistical parameters

When statistical analyses are reported, confirm that the following items are present in the relevant location (e.g. figure legend, table legend, main text, or Methods section).

n/a	Confirmed	
☐	☒	The <u>exact sample size</u> (*n*) for each experimental group/condition, given as a discrete number and unit of measurement
☐	☒	An indication of whether measurements were taken from distinct samples or whether the same sample was measured repeatedly
☐	☒	The statistical test(s) used AND whether they are one- or two-sided *Only common tests should be described solely by name; describe more complex techniques in the Methods section.*
☒	☐	A description of all covariates tested
☐	☒	A description of any assumptions or corrections, such as tests of normality and adjustment for multiple comparisons
☐	☒	A full description of the statistics including <u>central tendency</u> (e.g. means) or other basic estimates (e.g. regression coefficient) AND <u>variation</u> (e.g. standard deviation) or associated <u>estimates of uncertainty</u> (e.g. confidence intervals)
☐	☒	For null hypothesis testing, the test statistic (e.g. *F*, *t*, *r*) with confidence intervals, effect sizes, degrees of freedom and *P* value noted *Give P values as exact values whenever suitable.*
☒	☐	For Bayesian analysis, information on the choice of priors and Markov chain Monte Carlo settings
☒	☐	For hierarchical and complex designs, identification of the appropriate level for tests and full reporting of outcomes
☒	☐	Estimates of effect sizes (e.g. Cohen's *d*, Pearson's *r*), indicating how they were calculated
☐	☒	Clearly defined error bars *State explicitly what error bars represent (e.g. SD, SE, CI)*

Our web collection on <u>statistics for biologists</u> may be useful.

Software and code

Policy information about <u>availability of computer code</u>

Data collection	MATLAB (R2015a,R2016a), Psych toolbox (v. 3), Plexon recorder (v.2.3), Bruker's Prairie software (v.5.3), MultiClamp (v.700b), pClamp (v.10), Leica Application Suite X (v.3.1.5.16308), LifeCam Software Microsoft (v.3.60.253.0)
Data analysis	MATLAB (R2015a,R2016a), Plexon Offline Sorter (v.2.8.8), Mountain Sort Algorithm (v.1.0.0), ImageJ (v.1.48), Clampfit (v.10.4)

For manuscripts utilizing custom algorithms or software that are central to the research but not yet described in published literature, software must be made available to editors/reviewers upon request. We strongly encourage code deposition in a community repository (e.g. GitHub). See the Nature Research <u>guidelines for submitting code & software</u> for further information.

Data

Policy information about <u>availability of data</u>

All manuscripts must include a <u>data availability statement</u>. This statement should provide the following information, where applicable:
- Accession codes, unique identifiers, or web links for publicly available datasets
- A list of figures that have associated raw data
- A description of any restrictions on data availability

Data available on request from the authors

Field-specific reporting

Please select the best fit for your research. If you are not sure, read the appropriate sections before making your selection.

☒ Life sciences ☐ Behavioural & social sciences ☐ Ecological, evolutionary & environmental sciences

For a reference copy of the document with all sections, see nature.com/authors/policies/ReportingSummary-flat.pdf

Life sciences study design

All studies must disclose on these points even when the disclosure is negative.

Sample size	No statistical methods were used to pre-determine sample size. We used sample sizes similar to literature in the field. For all experiments, we also used sample sizes to provide at least 80% power to detect an effect.
Data exclusions	For single unit recording in the LC: Upon completion of experiments, we verified that targeting of the locus coeruleus region was successful with immunohistochemical techniques. Experiments where electrodes, fiber optics or viral delivery were mis-targeted were excluded from analysis. Recordings session with no ChR2 responsive units were also excluded from the study. We selected portion of extracellular single unit recordings where no obvious drift was detected.
	For slice electrophysiology: Recordings with a variation of access resistance greater than 15% were exclude.
	For pupillometry experiment: we excluded trials where baseline pupil size was hyper-dilated or constricted from analysis (<1st or >99th percentile of pupil size distribution).
	For histology using monosynaptic rabies tracing: Regions adjacent to LC were not considered for analysis due to non-specific expression of virus at the site of injection.
	These criteria were not pre-established.
Replication	All experiments were reproduced using biological replicates. Attempts at reproduction were successful. We used a range of 3 to 13 mice per conditions for each experiments.
Randomization	Auditory stimuli, and timing of optogenetics activation was randomized. Male or female mice were randomly selected for each experiment.
Blinding	Data collection and analysis was not performed blind. Sorting of neuronal type was performed after data collection.

Reporting for specific materials, systems and methods

Materials & experimental systems

n/a	Involved in the study
☒	☐ Unique biological materials
☐	☒ Antibodies
☒	☐ Eukaryotic cell lines
☒	☐ Palaeontology
☐	☒ Animals and other organisms
☒	☐ Human research participants

Methods

n/a	Involved in the study
☒	☐ ChIP-seq
☒	☐ Flow cytometry
☒	☐ MRI-based neuroimaging

Antibodies

Antibodies used	Primary antibodies: Chicken anti-tyrosine hydroxylase (TYH, Aves Labs, lot no. TYH8727985), dilution 1:1000 Rabbit anti-VGAT (131002, Synaptic Systems, lot no. 131002/34), dilution 1:1000 Rabbit anti-GABA (A2052, Sigma, lot no. 126M4791V), dilution 1:1000 Mouse anti-GAD67 (MAB5406 EMD Millipore, lot no. 2923238), dilution 1:200 Rabbit anti-neuropeptide S (ab18252 Abcam), dilution 1:500 Secondary antibodies Streptavidin-488 conjugated antibodies (S32354 ThermoFisher Scientific), dilution 1:200 Goat anti-chicken 647 nm (A21449, ThermoFisher Scientific), dilution 1:500 Goat anti-chicken 488 nm (A11039, ThermoFisher Scientific), dilution 1:500 Goat anti-rabbit 488 nm (A11034, ThermoFisher Scientific), dilution 1:500 Goat anti-mouse 488 nm (A21121, ThermoFisher Scientific), dilution 1:500

Validation	Chicken anti-tyrosine hydroxylase (TYH, Aves Labs) Validated in: Carter, M.E., et al. Tuning arousal with optogenetic modulation of locus coeruleus neurons. Nature neuroscience 13, 1526-1533 (2010). Rabbit anti-VGAT (131002, Synaptic Systems), Validated in: Saunders A, Oldenburg IA, Berezovskii VK, Johnson CA, Kingery ND, Elliott HL, Xie T, Gerfen CR & Sabatini BL (2015). A direct GABAergic output from the basal ganglia to frontal cortex. Nature 521: 85-9. 131 011; Rabbit anti-GABA (A2052, Sigma) Validated. R.O. Tasan, A. Bukovac,a Y.N. Peterschmitt, S.B. Sartori, R. Landgraf, N. Singewald, and G. Sperka Altered GABA transmission in a mouse model of increased trait anxiety. Neuroscience. 2011 Jun 2; 183(7): 71–80. Mouse anti-GAD67 (MAB5406 EMD Millipore) Validated in J Dimidschstein, Q Chen, R Tremblay, SL Rogers, GA Saldi, et. al. A viral strategy for targeting and manipulating interneurons across vertebrate species. Nature Neuroscience 2016 Dec; 19(2): 1743-1749. Rabbit anti-neuropeptide S (ab18252 Abcam) Validated in X Liu, J Zeng, A Zhou, E Theodorsson, J Fahrenkrug, RK Reinscheid. Molecular fingerprint of neuropeptide S-producing neurons in the mouse brain. J Comp Neurol. 2011 Jul 1;519(10):1847-66.

Animals and other organisms

Policy information about studies involving animals; ARRIVE guidelines recommended for reporting animal research

Laboratory animals	Adult mice (> 2 month old) of either sex were used in this study. We used the following mouse lines for the specific expression of various viruses in noradrenergic, GABAergic: TH-Cre (B6.Cg-Tg(Th-cre)1Tmd/J, Jackson Laboratory), Dbh-Cre (B6.FVB(Cg)-Tg(Dbh-cre)KH212Gsat/Mmucd, MMRRC), , GAD2-Cre (Gad2tm2(cre)Zjh/J, Jackson Laboratory). C57Bl/6 wild-type mice were used for control experiments. Optogenetic activation of LC GABAergic neurons (LC-GABA) was done also on VGAT-YFP-ChR2 (B6.Cg-Tg(Slc32a1-COP4*H134R/EYFP)8Gfng/J, Jackson Laboratory).
Wild animals	This study does not involve wild animals.
Field-collected samples	This study does not include field-collected samples.